Anyonic Phase Transitions in the 1D Extended Hubbard Model with Fractional Statistics

Martin Bonkhoff,[1,2] Kevin Jägering,[1] Shijie Hu,[1,3] Axel Pelster,[1] Sebastian Eggert,[1] and Imke Schneider[1]
[1]*Physics Department and Research Center OPTIMAS, University of Kaiserslautern-Landau, 67663 Kaiserslautern, Germany*
[2]*I. Institut für Theoretische Physik, Universität Hamburg, 22607 Hamburg, Germany*
[3]*Beijing Computational Science Research Center, Beijing 100193, China*

(Received 30 July 2024; revised 13 April 2025; accepted 16 June 2025; published 14 July 2025)

We study one-dimensional lattice anyons with extended Hubbard interactions at unit filling using bosonization and numerical simulations. The behavior can be continuously tuned from bosonic to fermionic statistics by adjusting the topological exchange angle θ, which leads to a competition of different instabilities. We present the bosonization theory in the presence of dynamic gauge fields, which predicts a phase diagram of four different gapped phases with distinct dominant correlations. Advanced numerical simulations determine and analyze the exact phase transitions between Mott insulator, charge density wave, dimerized state, and Haldane insulator, all of which meet at a multicritical line in the parameter space of anyonic angle θ, on-site interaction U, and nearest neighbor repulsion V. Superfluid and pair-superfluid phases are stable in a region of small V.

DOI: 10.1103/7n1c-vq2p

Introduction—For continuous one-dimensional (1D) systems an exotic particle species interpolating between bosons and fermions was first proposed by Leinaas and Myrheim [1,2]. This concept of anyons has received renewed interest with the implementation by so-called "lattice anyons" [3–17] based on experimental progress to create artificial gauge fields by dynamic manipulations and Floquet driving in ultracold gases [15–25], by Raman assisted coupling [26,27] or by impurities in 1D spin-charge separated systems [28]. The originally proposed continuous 1D anyons [1] correspond to the limit of low filling of interacting lattice anyons [29]. However, for unit filling of one particle per site strong lattice effects give rise to a completely different situation, where several broken symmetry phases are possible, which is the topic of this Letter. This is motivated by the observation that different instabilities have been established for fermions and bosons in the 1D extended Hubbard model at unit filling. In particular, the competition of on-site U and nearest neighbor V interactions leads to a possible dimerized (or bond ordered) phase for fermions [30–33], while for bosons topological string correlations in the form of a Haldane insulator (HI) are observed in an intermediate regime [34–37]. This invites the question for anyons: what is the nature of an intermediate phase as the anyonic exchange phase θ is tuned continuously between bosonic behavior for $\theta = 0$ to fermionic behavior for $\theta = \pi$? The goal of this Letter is to examine the transitions between all different instabilities and determine the dominant correlations as a function of θ, U, and V at unit filling.

The 1D extended Hubbard model for anyons can be written in standard notation as

$$\hat{H} = \sum_l \left[-J \hat{a}_l^\dagger \hat{a}_{l+1} + \text{H.c.} + \frac{U}{2} \hat{n}_l (\hat{n}_l - 1) + V \hat{n}_l \hat{n}_{l+1} \right]. \tag{1}$$

The anyonic statistics enters via the exchange phase θ in the deformed commutation relations on different sites $l \neq l'$: $\hat{a}_l \hat{a}_{l'}^\dagger - e^{i\theta \text{sgn}(l-l')} \hat{a}_{l'}^\dagger \hat{a}_l = 0$. Using a generalized Jordan-Wigner transformation $\hat{a}_l = \hat{b}_l \exp(i\theta \sum_{j<l} \hat{n}_j)$ [6] the anyonic model can be mapped to a bosonic one $[\hat{b}_{l'}^\dagger, \hat{b}_l] = 0$ for $l \neq l'$ with density-dependent hopping

$$\hat{H}_{\text{kin}} = -J \sum_l \left[\hat{b}_l^\dagger \hat{b}_{l+1} e^{i\theta \hat{n}_l} + \text{H.c.} \right]. \tag{2}$$

The on-site commutator $l = l'$ depends on the physical implementation, which is typically spinless bosons restricted to a maximum of two particles per site [7]. The limit of $\theta = \pi$ corresponds to spinless "pseudo-fermions" with the same on-site behavior but anticommutation relations for $l \neq l'$. We now derive the corresponding low-energy field theory, which will allow for drawing conclusions about the expected phase transitions.

Bosonization of gauge fields—For the constraint of maximally two particles per site at average unit filling, an exact representation can be used in terms of spin-1 operators $\hat{S}^z_l = -\hat{n}_l + 1$ which take on eigenvalues $-1, 0, 1$ [38]. The operations of the transformed hopping operator are given in terms of spin operators $\hat{S}^+_l|-1\rangle = \sqrt{2}|0\rangle$ and $\hat{S}^+_l|0\rangle = \sqrt{2}|1\rangle$ as

$$\hat{H}_{\mathrm{kin}} = -\frac{1}{2}\sum_l \left[t(\hat{S}^z_l, \hat{S}^z_{l+1})\hat{S}^-_l\hat{S}^+_{l+1} + \mathrm{H.c.}\right], \tag{3}$$

where the effective hopping is $t(-1,0) = 2Je^{i\theta}$, $t(0,1) = J$, $t(-1,1) = \sqrt{2}Je^{i\theta}$, and $t(0,0) = \sqrt{2}J$. A similar parametrization for interacting bosons has been used before [35] with the simplification $t = J$. Here we keep the full expression for t to avoid an artificial spin-flip symmetry and implement the θ-dependence, which can be written in terms of spin-operators as

$$t(\hat{S}^z_l, \hat{S}^z_{l+1}) = J\left[1 + d(\theta)\hat{S}^z_l\right]\left[1 + d(0)(\hat{S}^z_{l+1} - 1)\right], \tag{4}$$

with $d(\theta) = 1 - \sqrt{2}e^{i\theta}$. Following Refs. [35,39], we represent the spin-1 degrees of freedom by triplet states of two spin-$\frac{1}{2}$ operators, $\hat{S}^\pm_l = \hat{S}^\pm_{1,l} + \hat{S}^\pm_{2,l}$ and $\hat{S}^z_l = \hat{S}^z_{1,l} + \hat{S}^z_{2,l}$, for each site. This results in a spin-$\frac{1}{2}$ two-leg ladder model:

$$\begin{aligned}\hat{H}_{\mathrm{kin}} = -\frac{1}{2}\sum_l \Big[&\tilde{t}\Big(\hat{S}^z_{2,l}, \hat{S}^z_{2,l+1}\Big)\hat{S}^-_{1,l}\hat{S}^+_{1,l+1} \\ &+ \tilde{t}\Big(\hat{S}^z_{2,l}, \hat{S}^z_{1,l+1}\Big)\hat{S}^-_{1,l}\hat{S}^+_{2,l+1} \\ &+ \text{all terms with } 1 \leftrightarrow 2 + \mathrm{H.c.}\Big],\end{aligned} \tag{5}$$

where $1 \leftrightarrow 2$ denotes the interchange of chain indices 1 and 2 and $\tilde{t}(\hat{S}^z_{i,l}, \hat{S}^z_{j,l+1}) \equiv t(\hat{S}^z_{i,l} - 1/2, \hat{S}^z_{j,l+1} + 1/2)$ for i, $j = 1, 2$. Note that hopping in chain 1 depends on the spin operators $\hat{S}^z_{2,l}$ in chain 2, and vice versa. In that sense we may speak of a lattice gauge function [40]

$$\tilde{t}(\hat{S}^z_{i,l}, \hat{S}^z_{j,l+1}) = \tilde{J} + J_z\hat{S}^z_{i,l} + \bar{J}_z\hat{S}^z_{j,l+1} + J_{zz}\hat{S}^z_{i,l}\hat{S}^z_{j,l+1}, \tag{6}$$

with $\tilde{J} = (J/4)(1+\sqrt{2})(1+\sqrt{2}e^{i\theta})$ and higher spin interaction constants $J_z = (J/2)(1+\sqrt{2})(1-\sqrt{2}e^{i\theta})$, $\bar{J}_z = (J/2)(1-\sqrt{2})(1+\sqrt{2}e^{i\theta})$, and $J_{zz} = J(1-\sqrt{2})(1-\sqrt{2}e^{i\theta})$.

For low energies, the Hamiltonian of the coupled spin chains is expressed in terms of dual bosonic fields Θ_n and Φ_n for each chain $n = 1, 2$, which are defined for a continuum variable normalized such that $[\Phi_n(x), \Theta_{n'}(x')] = (i/2)\delta_{n,n'}\mathrm{sgn}(x - x')$ [35,41]. More details are given in Supplemental Material [40]. The resulting Hamiltonian is

$$\begin{aligned}\hat{H} \simeq \int dx \Bigg[&\sum_{\nu=+,-}\frac{u_\nu}{2}\left(K_\nu(\partial_x\Theta_\nu)^2 + K_\nu^{-1}(\partial_x\Phi_\nu)^2\right) \\ &+ \Delta(\partial_x\Theta_+\partial_x\Phi_+ + \partial_x\Theta_-\partial_x\Phi_-) \\ &+ g_1\cos\sqrt{4\pi}\Phi_+ + g_2\cos\sqrt{4\pi}\Phi_- \\ &+ g_3\cos\sqrt{4\pi}\Theta_- + g_4\cos\sqrt{4\pi}\Phi_+\cos\sqrt{4\pi}\Phi_-\Bigg],\end{aligned} \tag{7}$$

which we discuss below. Here $\Phi_\pm = \Phi_1 \pm \Phi_2$ and $\Theta_\pm = (\Theta_1 \pm \Theta_2)/2$ are the fields for the total $(+)$ and relative $(-)$ densities and phases of the two spin-$1/2$ chains, respectively. Terms which only affect conserved quantum numbers have been omitted. The parameters in the Hamiltonian can be determined in a weak-coupling expansion for small U, V, J_z, $\bar{J}_z$, and J_{zz}:

$$K_+ = 2\left[1 + \frac{6V + U - 4\mathrm{Re}J_{zz}/\pi}{\mathrm{Re}(\pi\tilde{J} - J_{zz}/2\pi)}\right]^{-1/2}, \tag{8}$$

$$K_- = 2\left[1 + \frac{2V - U - 4\mathrm{Re}J_{zz}/\pi}{\mathrm{Re}(\pi\tilde{J} - J_{zz}/2\pi)}\right]^{-1/2}, \tag{9}$$

$$u_\nu = 2a\mathrm{Re}(\tilde{J} - J_{zz}/2\pi^2)/K_\nu, \tag{10}$$

$$\Delta = -\frac{a}{\pi}\mathrm{Im}(J_z + \bar{J}_z) = \frac{2Ja}{\pi}\sin\theta, \tag{11}$$

$$\frac{g_1}{a} = \frac{1}{2}(2V - U) + \frac{2\mathrm{Re}(J_{zz})}{\pi}, \tag{12}$$

$$\frac{g_2}{a} = \frac{1}{2}(U - 2V) + \frac{2\mathrm{Re}(J_{zz})}{\pi}, \tag{13}$$

$$\frac{g_3}{a} = -\mathrm{Re}(\tilde{J})\pi, \tag{14}$$

$$\frac{g_4}{a} = V - \frac{\mathrm{Re}(J_{zz})}{\pi}, \tag{15}$$

where a is the lattice constant. Those expressions follow from a first order expansion in the interaction parameters and an operator product expansion [42,43] of the θ-dependent hopping terms as discussed in Supplemental Material [40]. However, the mapping from bosons to spin operators already implies a finite value $J_{zz} \neq 0$ even for $\theta = U = V = 0$, so the exact weak-coupling limit cannot be realized in the phase diagram. Hence, the actual coupling constants quantitatively differ from the formulas given above, but the operator content and the qualitative behavior with increasing θ, V and U are robust.

For $\theta = 0$ and $\tilde{t} = J$ we recover the structure and phases for bosons as discussed in Ref. [35]. For $\theta > 0$ we notice the appearance of a characteristic anyonic current-density interaction Δ on the second line in the Hamiltonian in Eq. (7). This term is present for any filling and leads to different left- and right-moving velocities [29]. While the corresponding time-dependent correlation functions now show chiral behavior, remarkably the static mode expansions of the fields remain unaffected [29], so scaling dimensions and the renormalization behavior are not changed by Δ.

Phase transitions—Next, we turn to the cosine interactions g_1, g_2, g_3, g_4 on the last two lines of the Hamiltonian in Eq. (7), all of which may be relevant and lead to gapped phases, depending on K_ν [35]. Notably, however, the $\sin\sqrt{4\pi}\Phi_+$ term is absent, even though spatial inversion symmetry $\mathcal{I}$ is broken [35]. This is due to the fact that a modified inversion symmetry $\tilde{\mathcal{I}}$ is still obeyed as discussed in Ref. [8], which forbids this operator (see Supplemental Material [40] for a discussion of symmetries).

In the $(+)$ sector a pinning of the field Φ_+ may occur due to the g_1 interaction, which is relevant for $K_+ < 2$. This case is discussed in the following, while $K_+ > 2$ corresponds to superfluid phases with irrelevant g_1, which is considered in End Matter Appendix B. For relevant $g_1 < 0$ the renormalization flow fixes the value of $\Phi_+ = 0$, while it becomes $\Phi_+ = \sqrt{\pi}/2$ for $g_1 > 0$, with a phase transition at $g_1 = 0$, characterized by a free field of conformal charge $c = 1$ [35]. The relative quantum numbers in the $(-)$ channel will also be pinned with long-range correlations. Here, two interactions $g_2 < 0$ and $g_3 < 0$ compete with scaling dimensions of K_- and $1/K_-$, respectively. The renormalization flow for $K_- < 1$ will lead to a minimum at $\Phi_- = 0$, while $K_- > 1$ is characterized by $\Theta_- = 0$. The phase transition for $K_- = 1$ is predicted to be in the Ising universality class with $c = 1/2$ as long as $g_2 \approx g_3$ [35,44]. For the model at hand a sign change of g_2 is only possible where it is not the leading instability. The two phase transitions are plotted schematically in Fig. 1 by using the conditions $g_1 = 0$ and $K_- = 1$ to determine a critical U^c as a function of $-\mathrm{Re}J_{zz} \propto 1 - \sqrt{2}\cos\theta$ for a fixed value of V. From Eqs. (8)–(15) we get the weak-coupling limit

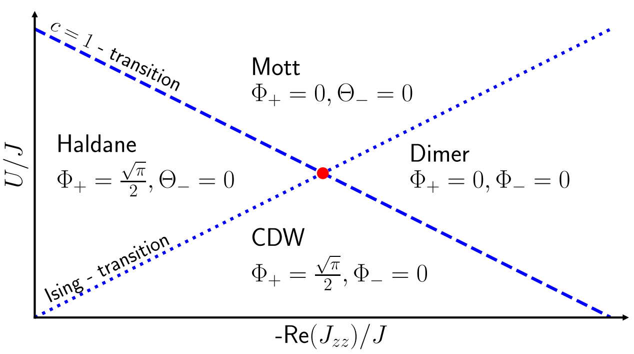

FIG. 1. Schematic phase diagram resulting from bosonization in Eqs. (16) and (17) as a function of U and $-\mathrm{Re}J_{zz} \propto 1 - \sqrt{2}\cos\theta$ for fixed V and $\tilde{J}$. At one point (red) four gapped phases meet, each of which is characterized by the minimum values of bosonic fields.

$$U^{\mathrm{c}}_{c=1}(\theta) \sim 2V + \frac{4\mathrm{Re}[J_{zz}(\theta)]}{\pi} \tag{16}$$

$$U^{\mathrm{c}}_{\mathrm{Ising}}(\theta) \sim 2V - \frac{5\mathrm{Re}[J_{zz}(\theta)]}{2\pi} - 3\pi\mathrm{Re}[\tilde{J}(\theta)]. \tag{17}$$

For $\theta = 0$ the corresponding long-range ($|i-j| \to \infty$) order parameters have been discussed in Ref. [35] in terms of densities $\delta\hat{n}_l = \hat{n}_l - 1$ and fields $\Phi_\pm$. For $U > U^{\mathrm{c}}_{c=1} > U^{\mathrm{c}}_{\mathrm{Ising}}$ the pinning $\Phi_+ = \Theta_- = 0$ corresponds to the Mott insulator (MI) with parity order parameter

$$\mathcal{O}^2_{\mathrm{MOTT}} = \langle \mathrm{e}^{i\pi\sum_{i<k<j}\delta\hat{n}_k}\rangle \sim (\cos\sqrt{\pi}\Phi_+)^2, \tag{18}$$

while $U^{\mathrm{c}}_{c=1} > U^{\mathrm{c}}_{\mathrm{Ising}} > U$ is a charge density wave (CDW) with alternating charge order $\Phi_+ = \sqrt{\pi}/2$ and fixed relative densities $\Phi_- = 0$ characterized by long-range density correlations

$$\mathcal{O}^2_{\mathrm{CDW}} = (-1)^{|i-j|}\langle\delta\hat{n}_i\delta\hat{n}_j\rangle \sim (\sin\sqrt{\pi}\Phi_+\cos\sqrt{\pi}\Phi_-)^2. \tag{19}$$

Alternatively, a local order parameter $\mathcal{O}_{\mathrm{CDW}}$ can be defined as the even-odd density difference, which manifests the breaking of the $\mathbb{Z}_2$ symmetry with respect to bond-centered inversion [40]. In the intermediate case, $U^{\mathrm{c}}_{c=1} > U > U^{\mathrm{c}}_{\mathrm{Ising}}$, a Haldane insulating phase has been identified with alternating local charge $\Phi_+ = \sqrt{\pi}/2$ but fluctuating relative densities $\Theta_- = 0$ and topological string order parameter

$$\mathcal{O}^2_{\mathrm{HI}} = \langle\delta\hat{n}_i \mathrm{e}^{i\pi\sum_{i\le k<j}\delta\hat{n}_k}\delta\hat{n}_j\rangle \sim (\sin\sqrt{\pi}\Phi_+)^2. \tag{20}$$

For larger θ, anyons now open another possibility for the intermediate phase, as $U^{\mathrm{c}}_{\mathrm{Ising}}$ increases and $U^{\mathrm{c}}_{c=1}$ decreases with θ, such that $U^{\mathrm{c}}_{c=1} < U < U^{\mathrm{c}}_{\mathrm{Ising}}$, which is not possible for bosons. In this case the order parameter is given by alternating energies on even and odd bonds as

$$\mathcal{O}_{\mathrm{DIMER}} = \langle\hat{H}^{\mathrm{bond}}_{\mathrm{even}} - \hat{H}^{\mathrm{bond}}_{\mathrm{odd}}\rangle \sim \cos\sqrt{\pi}\Phi_+\cos\sqrt{\pi}\Phi_-, \tag{21}$$

corresponding to uniform local charges $\Phi_+ = 0$ with relative quantum numbers entangled on every second bond $\Phi_- = 0$. For the Fermionic Hubbard model the dimer phase is also known as a bond ordered wave [31]. However, it is not trivial that such a phase is now also observed for $\theta = \pi$ corresponding to "pseudo-fermions" where the on-site commutator is bosonic with at most two particles per site. The Fermionic Hubbard model has a local Hilbert state of four states per site, while the model in Eq. (1) is restricted to three states, where the relative densities in the $(-)$ channel play the role of fermionic spins.

Numerical results—The density matrix renormalization group (DMRG) algorithm [45,46] and the infinite DMRG (iDMRG) [47] with $M = 100$–800 kept states were used to calculate the fidelity susceptibility, the entanglement

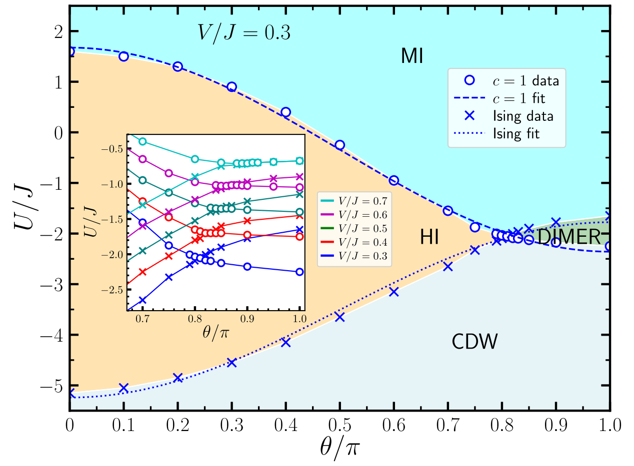

FIG. 2. Phase diagram as a function of θ and U/J for $V/J = 0.3$ obtained by fidelity susceptibility from iDMRG with bond dimension $M = 400$. Circles denote the $c = 1$ transition, and crosses show the Ising transition. The dashed and dotted lines are fits to Eqs. (16) and (17), respectively (see text). Inset: behavior near the points, where all four phases meet for different V/J.

entropy, order parameters, and the correlation length, as well as level spectroscopy with finite-size scaling. The fidelity susceptibility provides a robust sharp signal and has been used to obtain the phase boundaries between the four gapped phases in Figs. 2 and 3, which agree with maxima of the other quantities using an accuracy of parameter spacing $0.1J$. See End Matter Appendix A for a more detailed discussion of the numerical approach.

The bosonization results in Eqs. (16) and (17) predict a $\cos\theta$ dependence of the phase transition lines of the form $(U^{c}_{c=1}(\theta) - U^{c}_{c=1}(\pi/2))/J = a\cos\theta$ and $(U^{c}_{\mathrm{Ising}}(\theta) - U^{c}_{\mathrm{Ising}}(\pi/2))/J = b\cos\theta$, where the weak-coupling expressions evaluate to $a \sim 0.74$ and $b \sim -8.5$ with opposite signs. Due to finite coupling values those prefactors renormalize, but the cos behavior appears to be robust, as can be seen by the fits of the phase transition lines in Fig. 2, which are given by $U^{c}_{c=1}/J = -0.34 + 2.02\cos\theta$ and $U^{c}_{\mathrm{Ising}}/J = -3.51 - 1.73\cos\theta$.

The inset of Fig. 2 shows the behavior near the points where all four phases meet for different V. For each fixed V, the phase transition lines cross, which would signal the appearance of a four-critical point between the MI, HI, CDW, and dimer phases. According to bosonization the multicritical point would have central charge $c = 3/2$ [48]. All data is consistent with four phases meeting exactly at one multicritical line in the U-V-θ parameter space.

More detailed phase diagrams in the U-V-parameter space for different θ are presented in Fig. 3. The width of the HI phase has considerably decreased for $\theta = \pi/2$, and for $\theta = 3\pi/4$ it is almost gone. For $\theta = \pi$ the HI phase is completely replaced by a dimer phase consistent with the prediction by bosonization. For large V the intermediate phase always merges into a first order transition between Mott and CDW phases. The dimer phase extends to negative U over a larger region than for the Fermionic Hubbard model [31].

An interesting aspect for small values of V is the appearance of a superfluid (SF) for bosons and a pair-superfluid (PSF) phase for both bosons and pseudofermions in the insets of Fig. 3. For $V = 0$ the behavior was analyzed numerically in Ref. [7], which can now be explained in terms of our bosonization approach at unit filling. In particular, superfluid behavior requires an irrelevant coupling g_1 in the $(+)$ sector $K_+ > 2$, i.e., $U + 6V - 4\mathrm{Re}(J_{zz})/\pi < 0$ from the weak coupling limit in Eq. (8). Accordingly, superfluid behavior is possible even for positive regions of U at $V = 0$ due to the fact that $J_{zz}(\theta = 0) > 0$, which would not be the case if an artificial spin-flip symmetry was assumed as in previous works. With increasing θ the critical value of U decreases since $\mathrm{Re}(J_{zz}) \propto \sqrt{2}\cos\theta - 1$, which is exactly observed numerically in Ref. [7]. The SF-PSF transition is discussed in End Matter Appendix B, where it is shown that it corresponds to $K_- = 1$. As can be seen in the inset of Fig. 3 it is therefore a continuation of the Ising transition discussed above, where it was predicted that the $K_- = 1$ transition occurs at larger values of U with increasing θ. Hence, with larger θ eventually the decreasing $K_+ = 2$ and the increasing $K_- = 1$ lines cross, which marks a multicritical point where the

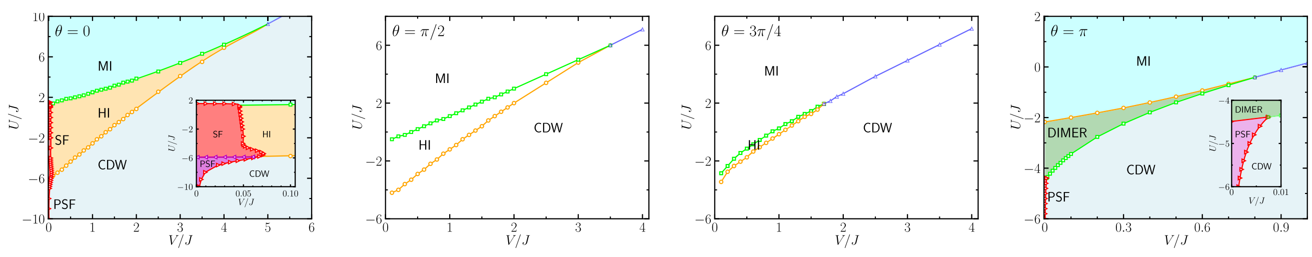

FIG. 3. Phase diagram as a function of U/J and V/J showing the fate of the intermediate phase at $\theta = 0$, $\theta = \pi/2$, $\theta = 3\pi/4$, and $\theta = \pi$ (from left to right), numerically determined by the maxima of the fidelity susceptibility using iDMRG. Green ($c = 1$) and yellow (Ising) denote continuous transition lines, and blue is first order. Insets: for $\theta = 0$ and $\theta = \pi$, close-up of the superfluid and pair-superfluid behavior determined by level spectroscopy (red lines, see End Matter Appendix B).

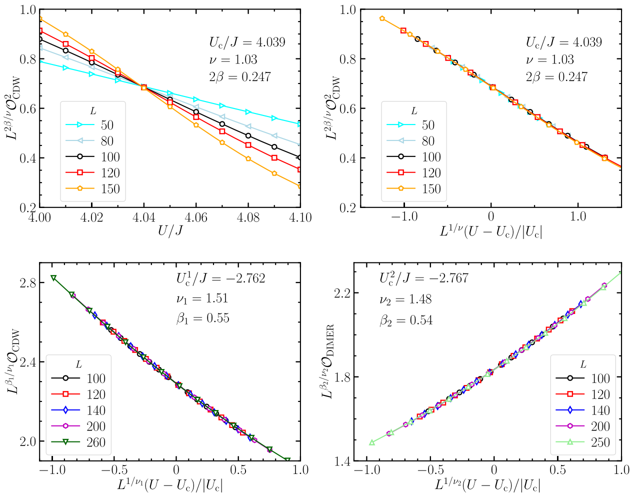

FIG. 4. Finite size L scaling analysis of the order parameters from DMRG. Upper: data collapse of $\mathcal{O}^2_{\mathrm{CDW}}$ along the HI-CDW transition at $V/J = 3$, $\theta = 0$. Lower: data collapse of $\mathcal{O}_{\mathrm{CDW}}$ (density difference) (lower left) and $\mathcal{O}_{\mathrm{DIMER}}$ (lower right) along the CDW-dimer transition at $V/J = 0.2$, $\theta = \pi$.

SF phase is replaced by the dimer phase at $\theta \sim 0.8\pi$ for $V = 0$ as first shown in Ref. [7]. More details on the superfluid phases are discussed in End Matter Appendix B.

Classification of transitions—For the determination of universality classes the scaling of the order parameters is analyzed, which is numerically more involved (see Supplemental Material [40]). This is illustrated in Fig. 4 (upper) for the transition between the HI and CDW phases. The data collapse gives an accurate determination of critical exponents $\nu = 1.03$ and $2\beta = 0.247$. This is in agreement with the prediction of an Ising transition with $c = 1/2$ [8,35], which we confirmed by entanglement entropy scaling [49] in the insets of Fig. 5 in End Matter Appendix A.

More interesting is the transition from CDW to dimer phase. Both phases show a spontaneously broken translation symmetry but different broken inversion symmetries: bond centered and site centered, respectively. Recent literature has extensively discussed continuous transitions between two phases with different broken $\mathbb{Z}_2$ symmetries as interesting examples [48,50–59] beyond the Landau-Ginzburg paradigm [60] in connection with deconfined quantum criticality [57–59]. While in two-dimensional systems numerical evidence for a continuous transition is hard to obtain [61,62], the one-dimensional system now offers more controlled methods. For the anyon model we can confirm that the CDW-dimer transition also falls in this remarkable category. It is continuous at $V/J = 0.2$, $\theta = \pi$ for a $c = 1$ transition as shown in Fig. 4 (lower). From bosonization this can be understood because the sign change of g_1 causes the $c = 1$ transition and at the same time a change of the $\mathbb{Z}_2$ symmetry of the respective order parameter, interchanging the role of $\cos\sqrt{\pi}\Phi_+$ and $\sin\sqrt{\pi}\Phi_+$ in Eqs. (19) and (21). See Supplemental Material [40] for a discussion of symmetries.

For the extended Bose Hubbard model, the HI to Mott transition is known to be $c = 1$ [36,37,63]. It is weaker for small V [8] and merges to a first order Mott-CDW transition for large V as shown in Fig. 3. We observe no significant change in the nature of the transition for finite θ. A coupling in the form of the operator $\sin\sqrt{4\pi}\Phi_+$ is therefore always absent, which would otherwise lead to a crossover behavior instead of a sharp $c = 1$ line [35].

Finally, all transitions between the (pair) superfluid phases and the gapped phases are of Berezinskii-Kosterlitz-Thouless (BKT) type (red lines in the insets of Fig. 3). As discussed in End Matter Appendix B, the corresponding transition lines were established using level spectroscopy [64–70] with exact diagonalization for finite-size systems extrapolated to the thermodynamic limit.

Conclusions—By derivation of the effective field theory and large scale numerical DMRG calculations we have obtained the phase diagram as a function of θ, U, and V of the extended anyonic Hubbard model including negative on-site interactions. The phase diagram consists of four gapped and two superfluid phases. By tuning the exchange angle θ from 0 to π the behavior changes continuously from bosonic to fermionic. In the process the Haldane insulator phase disappears at an interesting multicritical point where it is replaced by the dimer phase. The transition between dimer and CDW phases provides an example of a continuous $c = 1$ transition between two distinct broken $\mathbb{Z}_2$ symmetries beyond the Landau-Ginzburg paradigm.

Acknowledgments—We thank Nicholas Sedlmayr, Thore Posske, Sebastian Greschner, Pascal Jung, and Nathan Harshman for helpful discussions. We acknowledge support from the Deutsche Forschungsgemeinschaft (DFG, German Research Foundation) Project No. 277625399-TRR 185 OSCAR (A4,A5,B6) and DFG Forschungsgruppe FOR 2316 Project No. P10. S.-J. H. acknowledges funding from the Ministry of Science and Technology of the People's Republic of China under Grant No. 2022YFA1402700 and the National Natural Science Foundation of China under Grants No. U2230402 and No. 12174020.

[1] J. Leinaas and J. Myrheim, On the theory of identical particles, Nuovo Cimento Soc. Ital. Fis. **37B**, 1 (1977).

[2] In the original paper [1] fractional statistics for both two-dimensional and one-dimensional geometries are discussed. Our Letter refers to the 1D case.

[3] A. Eckardt, Colloquium: Atomic quantum gases in periodically driven optical lattices, Rev. Mod. Phys. **89**, 011004 (2017).

[4] N. Goldman and J. Dalibard, Periodically driven quantum systems: Effective Hamiltonians and engineered gauge fields, Phys. Rev. X **4**, 031027 (2014).

[5] M. Bukov, L. D'Alessio, and A. Polkovnikov, Universal high-frequency behavior of periodically driven systems: From dynamical stabilization to Floquet engineering, Adv. Phys. **64**, 139 (2015).
[6] T. Keilmann, S. Lanzmich, I. McCulloch, and M. Roncaglia, Statistically induced phase transitions and anyons in 1D optical lattices, Nat. Commun. **2**, 361 (2011).
[7] S. Greschner and L. Santos, Anyon Hubbard model in one-dimensional optical lattices, Phys. Rev. Lett. **115**, 053002 (2015).
[8] F. Lange, S. Ejima, and H. Fehske, Anyonic Haldane insulator in one dimension, Phys. Rev. Lett. **118**, 120401 (2017).
[9] C. Sträter, S. C. L. Srivastava, and A. Eckardt, Floquet realization and signatures of one-dimensional anyons in an optical lattice, Phys. Rev. Lett. **117**, 205303 (2016).
[10] G. Tang, S. Eggert, and A. Pelster, Ground-state properties of anyons in a one-dimensional lattice, New J. Phys. **17**, 123016 (2015).
[11] F. Lange, S. Ejima, and H. Fehske, Strongly repulsive anyons in one dimension, Phys. Rev. A **95**, 063621 (2017).
[12] J. Arcila-Forero, R. Franco, and J. Silva-Valencia, Critical points of the anyon-Hubbard model, Phys. Rev. A **94**, 013611 (2016).
[13] J. Arcila-Forero, R. Franco, and J. Silva-Valencia, Three-body-interaction effects on the ground state of one-dimensional anyons, Phys. Rev. A **97**, 023631 (2018).
[14] M. Bonkhoff, S. B. Jäger, I. Schneider, A. Pelster, and S. Eggert, Coherence properties of the repulsive anyon-Hubbard dimer, Phys. Rev. B **108**, 155134 (2023).
[15] F. Görg, K. Sandholzer, J. Minguzzi, R. Desbuquois, M. Messer, and T. Esslinger, Realization of density-dependent Peierls phases to engineer quantized gauge fields coupled to ultracold matter, Nat. Phys. **15**, 1161 (2019).
[16] V. Lienhard, P. Scholl, S. Weber, D. Barredo, S. de Léséleuc, R. Bai, N. Lang, M. Fleischhauer, H. P. Büchler, T. Lahaye, and A. Browaeys, Realization of a density-dependent Peierls phase in a synthetic, spin-orbit coupled Rydberg system, Phys. Rev. X **10**, 021031 (2020).
[17] J. Kwan, P. Segura, Y. Li, S. Kim, A. V. Gorshkov, A. Eckardt, B. Bakkali-Hassani, and M. Greiner, Realization of one-dimensional anyons with arbitrary statistical phase, Science **386**, 1055 (2024).
[18] I. Bloch, J. Dalibard, and W. Zwerger, Many-body physics with ultracold gases, Rev. Mod. Phys. **80**, 885 (2008).
[19] M. Aidelsburger, M. Atala, M. Lohse, J. T. Barreiro, B. Paredes, and I. Bloch, Realization of the Hofstadter Hamiltonian with ultracold atoms in optical lattices, Phys. Rev. Lett. **111**, 185301 (2013).
[20] H. Miyake, G. A. Siviloglou, C. J. Kennedy, W. C. Burton, and W. Ketterle, Realizing the Harper Hamiltonian with laser-assisted tunneling in optical lattices, Phys. Rev. Lett. **111**, 185302 (2013).
[21] J. Struck, M. Weinberg, C. Ölschläger, P. Windpassinger, J. Simonet, K. Sengstock, R. Höppner, P. Hauke, A. Eckardt, M. Lewenstein, and L. Mathey, Engineering Ising-XY spin-models in a triangular lattice using tunable artificial gauge fields, Nat. Phys. **9**, 738 (2013).
[22] S. Fazzini, P. Chudzinski, C. Dauer, I. Schneider, and S. Eggert, Nonequilibrium Floquet steady states of time-periodic driven Luttinger liquids, Phys. Rev. Lett. **126**, 243401 (2021).
[23] C. Schweizer, F. Grusdt, M. Berngruber, L. Barbiero, E. Demler, N. Goldman, I. Bloch, and M. Aidelsburger, Floquet approach to $\mathbb{Z}_2$ lattice gauge theories with ultracold atoms in optical lattices, Nat. Phys. **15**, 1168 (2019).
[24] T. Langen, R. Geiger, and J. Schmiedmayer, Ultracold atoms out of equilibrium, Annu. Rev. Condens. Matter Phys. **6**, 201 (2015).
[25] C. Gross and I. Bloch, Quantum simulations with ultracold atoms in optical lattices, Science **357**, 995 (2017).
[26] A. Frölian, C. S. Chisholm, E. Neri, C. R. Cabrera, R. Ramos, A. Celi, and L. Tarruell, Realizing a 1D topological gauge theory in an optically dressed BEC, Nature (London) **608**, 293 (2022).
[27] C. S. Chisholm, A. Frölian, E. Neri, R. Ramos, L. Tarruell, and A. Celi, Encoding a one-dimensional topological gauge theory in a Raman-coupled Bose-Einstein condensate, Phys. Rev. Res. **4**, 043088 (2022).
[28] S. Dhar, B. Wang, M. Horvath, A. Vashisht, Y. Zeng, M. B. Zvonarev, N. Goldman, Y. Guo, M. Landini, and H.-C. Nägerl, Observing anyonization of bosons in a quantum gas, Nature (London) **642**, 53 (2025).
[29] M. Bonkhoff, K. Jägering, S. Eggert, A. Pelster, M. Thorwart, and T. Posske, Bosonic continuum theory of one-dimensional lattice anyons, Phys. Rev. Lett. **126**, 163201 (2021).
[30] M. Nakamura, Mechanism of CDW-SDW transition in one dimension, J. Phys. Soc. Jpn. **68**, 3123 (1999).
[31] P. Sengupta, A. W. Sandvik, and D. K. Campbell, Bond-order-wave phase and quantum phase transitions in the one-dimensional extended Hubbard model, Phys. Rev. B **65**, 155113 (2002).
[32] A. W. Sandvik, L. Balents, and D. K. Campbell, Ground state phases of the half-filled one-dimensional extended Hubbard model, Phys. Rev. Lett. **92**, 236401 (2004).
[33] L. Barbiero, S. Fazzini, and A. Montorsi, Non-local order parameters as a probe for phase transitions in the extended Fermi-Hubbard model, Eur. Phys. J. Spec. Top. **226**, 2697 (2017).
[34] E. G. Dalla Torre, E. Berg, and E. Altman, Hidden order in 1D Bose insulators, Phys. Rev. Lett. **97**, 260401 (2006).
[35] E. Berg, E. G. Dalla Torre, T. Giamarchi, and E. Altman, Rise and fall of hidden string order of lattice Bosons, Phys. Rev. B **77**, 245119 (2008).
[36] S. Ejima, F. Lange, and H. Fehske, Spectral and entanglement properties of the Bosonic Haldane insulator, Phys. Rev. Lett. **113**, 020401 (2014).
[37] D. Rossini and R. Fazio, Phase diagram of the extended Bose Hubbard model, New J. Phys. **14**, 065012 (2012).
[38] M. Dalmonte, M. Di Dio, L. Barbiero, and F. Ortolani, Homogeneous and inhomogeneous magnetic phases of constrained dipolar Bosons, Phys. Rev. B **83**, 155110 (2011).
[39] H. J. Schulz, Phase diagrams and correlation exponents for quantum spin chains of arbitrary spin quantum number, Phys. Rev. B **34**, 6372 (1986).
[40] See Supplemental Material at http://link.aps.org/supplemental/10.1103/7n1c-vq2p for details about the lattice gauge function, bosonization, symmetry transformations, and behavior of the order parameter.

[41] T. Giamarchi, *Quantum Physics in One Dimension* (Clarendon Press, Oxford, 2003).
[42] P. Di Francesco, P. Mathieu, and D. Sénéchal, *Conformal Field Theory*, Graduate Texts in Contemporary Physics (Springer, New York, 1997).
[43] G. I. Japaridze and A. P. Kampf, Weak-coupling phase diagram of the extended Hubbard model with correlated-hopping interaction, Phys. Rev. B **59**, 12822 (1999).
[44] P. Lecheminant, A. O. Gogolin, and A. A. Nersesyan, Criticality in self-dual sine-Gordon models, Nucl. Phys. **B639**, 502 (2002).
[45] S. R. White, Density matrix formulation for quantum renormalization groups, Phys. Rev. Lett. **69**, 2863 (1992).
[46] S. R. White, Density-matrix algorithms for quantum renormalization groups, Phys. Rev. B **48**, 10345 (1993).
[47] I. P. McCulloch, Infinite size density matrix renormalization group, revisited, arXiv:0804.2509.
[48] T. Ogino, S. Furukawa, R. Kaneko, S. Morita, and N. Kawashima, Symmetry-protected topological phases and competing orders in a spin-$\frac{1}{2}$ XXZ ladder with a four-spin interaction, Phys. Rev. B **104**, 075135 (2021).
[49] S. Nishimoto, Tomonaga-Luttinger-liquid criticality: Numerical entanglement entropy approach, Phys. Rev. B **84**, 195108 (2011).
[50] R. A. Macêdo, F. B. Ramos, and R. G. Pereira, Continuous phase transition from a chiral spin state to collinear magnetic order in a zigzag chain with Kitaev interactions, Phys. Rev. B **105**, 205144 (2022).
[51] C. Mudry, A. Furusaki, T. Morimoto, and T. Hikihara, Quantum phase transitions beyond Landau-Ginzburg theory in one-dimensional space revisited, Phys. Rev. B **99**, 205153 (2019).
[52] S. Jiang and O. Motrunich, Ising ferromagnet to valence bond solid transition in a one-dimensional spin chain: Analogies to deconfined quantum critical points, Phys. Rev. B **99**, 075103 (2019).
[53] R.-Z. Huang, D.-C. Lu, Y.-Z. You, Z. Y. Meng, and T. Xiang, Emergent symmetry and conserved current at a one-dimensional incarnation of deconfined quantum critical point, Phys. Rev. B **100**, 125137 (2019).
[54] B. Roberts, S. Jiang, and O. I. Motrunich, Deconfined quantum critical point in one dimension, Phys. Rev. B **99**, 165143 (2019).
[55] Q. Luo, S. Hu, J. Li, J. Zhao, H.-Y. Kee, and X. Wang, Spontaneous dimerization, spin-nematic order, and deconfined quantum critical point in a spin-1 Kitaev chain with tunable single-ion anisotropy, Phys. Rev. B **107**, 245131 (2023).
[56] C. Zhang and M. Levin, Exactly solvable model for a deconfined quantum critical point in 1D, Phys. Rev. Lett. **130**, 026801 (2023).
[57] T. Senthil, L. Balents, S. Sachdev, A. Vishwanath, and M. P. A. Fisher, Quantum criticality beyond the Landau-Ginzburg-Wilson paradigm, Phys. Rev. B **70**, 144407 (2004).
[58] M. Levin and T. Senthil, Deconfined quantum criticality and Néel order via dimer disorder, Phys. Rev. B **70**, 220403(R) (2004).
[59] C. Wang, A. Nahum, M. A. Metlitski, C. Xu, and T. Senthil, Deconfined quantum critical points: Symmetries and dualities, Phys. Rev. X **7**, 031051 (2017).
[60] L. Landau and E. Lifshitz, *Statistical Physics, Part I*, Vol. 5 (Elsevier Butterworth-Heinemann, Oxford, 1980).
[61] J. D'Emidio, A. A. Eberharter, and A. M. Läuchli, Diagnosing weakly first-order phase transitions by coupling to order parameters, SciPost Phys. **15**, 061 (2023).
[62] M. Song, J. Zhao, M. Cheng, C. Xu, M. M. Scherer, L. Janssen, and Z. Y. Meng, Evolution of entanglement entropy at SU(n) deconfined quantum critical points, Sci. Adv. **11**, eadr0634 (2025).
[63] S. Ejima and H. Fehske, Comparative density-matrix renormalization group study of symmetry-protected topological phases in spin-1 chain and Bose-Hubbard models, Phys. Rev. B **91**, 045121 (2015).
[64] K. Okamoto and K. Nomura, Fluid-dimer critical point in $S = 1/2$ antiferromagnetic Heisenberg chain with next nearest neighbor interactions, Phys. Lett. A **169**, 433 (1992).
[65] S. Eggert, Numerical evidence for multiplicative logarithmic corrections from marginal operators, Phys. Rev. B **54**, R9612 (1996).
[66] S. Miyakoshi, S. Nishimoto, and Y. Ohta, Entanglement properties of the Haldane phases: A finite system-size approach, Phys. Rev. B **94**, 235155 (2016).
[67] L. Wang and A. W. Sandvik, Critical level crossings and gapless spin liquid in the square-lattice spin-1/2 $J_1 - J_2$ Heisenberg antiferromagnet, Phys. Rev. Lett. **121**, 107202 (2018).
[68] T. Wang, S. Hu, S. Eggert, M. Fleischhauer, A. Pelster, and X.-F. Zhang, Floquet-induced superfluidity with periodically modulated interactions of two-species hardcore bosons in a one-dimensional optical lattice, Phys. Rev. Res. **2**, 013275 (2020).
[69] P. Zhong, T. Wang, S. Hu, and H. Lin, Quantum phase diagram for two-species hardcore bosons in one-dimensional optical lattices with resonantly driven Rabi frequency, Phys. Rev. B **106**, 045130 (2022).
[70] J.-L. He, S. Eggert, H. Lin, X. Wang, and S. J. Hu, Competition between dimerization and vector chirality in the spin-3/2 $J_2 - J_2$ Heisenberg chain with uniaxial single-ion anisotropy, Phys. Rev. B **110**, 195129 (2024).
[71] W.-L. You, Y.-W. Li, and S.-J. Gu, Fidelity, dynamic structure factor, and susceptibility in critical phenomena, Phys. Rev. E **76**, 022101 (2007).
[72] P. Zanardi and N. Paunković, Ground state overlap and quantum phase transitions, Phys. Rev. E **74**, 031123 (2006).
[73] X. Wang, Boundary and impurity effects on the entanglement of Heisenberg chains, Phys. Rev. E **69**, 066118 (2004).
[74] A. Osterloh, L. Amico, G. Falci, and R. Fazio, Scaling of entanglement close to a quantum phase transition, Nature (London) **416**, 608 (2002).
[75] Q. Luo, S. Hu, B. Xi, J. Zhao, and X. Wang, Ground-state phase diagram of an anisotropic spin-$\frac{1}{2}$ model on the triangular lattice, Phys. Rev. B **95**, 165110 (2017).
[76] Q. Luo, S. Hu, J. Zhao, A. Metavitsiadis, S. Eggert, and X. Wang, Ground-state phase diagram of the frustrated spin-$\frac{1}{2}$ two-leg honeycomb ladder, Phys. Rev. B **97**, 214433 (2018).

[77] T. Sowiński, R. W. Chhajlany, O. Dutta, L. Tagliacozzo, and M. Lewenstein, Criticality in the Bose-Hubbard model with three-body repulsion, Phys. Rev. A **92**, 043615 (2015).
[78] N. Cuzzuol, L. Barbiero, and A. Montorsi, Nonlocal order parameter of pair superfluids, SciPost Phys. Core **8**, 020 (2025).
[79] A. J. Daley, J. M. Taylor, S. Diehl, M. Baranov, and P. Zoller, Atomic three-body loss as a dynamical three-body interaction, Phys. Rev. Lett. **102**, 040402 (2009).
[80] Y.-W. Lee and M.-F. Yang, Superfluid-insulator transitions in attractive Bose-Hubbard model with three-body constraint, Phys. Rev. A **81**, 061604(R) (2010).
[81] Y.-C. Chen, K.-K. Ng, and M.-F. Yang, Quantum phase transitions in the attractive extended Bose-Hubbard model with a three-body constraint, Phys. Rev. B **84**, 092503 (2011).
[82] L. Bonnes and S. Wessel, Pair superfluidity of three-body constrained Bosons in two dimensions, Phys. Rev. Lett. **106**, 185302 (2011).
[83] K.-K. Ng and M.-F. Yang, Thermal phase transitions in the attractive extended Bose-Hubbard model with three-body constraint, Phys. Rev. B **83**, 100511(R) (2011).

End Matter

Appendix A: Numerical data—For the numerical determination of the phase transition lines, we discuss the fidelity susceptibility, the entanglement entropy, and the correlation length here. Order parameters are discussed in Supplemental Material [40].

For determining the continuous transitions between gapped phases we use iDMRG [47] to calculate the fidelity F and its susceptibility χ_{F} [71,72]. The fidelity is defined as the absolute value of the overlap between a quantum state $|\Psi(\lambda)\rangle$ with a state with a slightly shifted parameter $|\Psi(\lambda+\delta\lambda)\rangle$, $\mathrm{F}(\delta\lambda)=|\langle\Psi(\lambda)|\Psi(\lambda+\delta\lambda)\rangle|$, from which the fidelity susceptibility is derived:

$$\chi_{\mathrm{F}}=-\frac{2\ln(\mathrm{F})}{\delta\lambda^2}. \tag{A1}$$

Here, λ is the parameter across which the phase transition is to be located, and $\delta\lambda$ is typically fixed around $0.05J$ to define the desired accuracy in parameter space.

Another useful quantity is the entanglement entropy,

$$S(\hat{\rho}_L)=-\mathrm{tr}\hat{\rho}_L\ln(\hat{\rho}_L), \tag{A2}$$

of the reduced density matrix $\hat{\rho}_L=\mathrm{tr}_R\hat{\rho}$ for the left subsystem, where the right part has been traced out [73–76]. At a gap-to-gap continuous phase transition, the entanglement entropy diverges logarithmically in the correlation length ξ when approaching a critical point [49] $S(\hat{\rho}_L)\propto c\ln(\xi)$ with c being the central charge of the underlying conformal field theory. For finite size systems the correlation length at the continuous transition is limited by the system size L. At the critical point, $S(\hat{\rho}_L)$ then diverges as

$$S(\hat{\rho}_L)=\frac{c}{6}\ln(L) \tag{A3}$$

for open boundary conditions [49]. With open boundary DMRG the entanglement entropy is alternating along the chain due to edge effects. The average of the larger S^{str} and smaller S^{weak} values determines c in the thermodynamic limit shown in the insets of Fig. 5.

The correlation length ξ shows a pronounced maximum near phase transitions. Instead of calculating the density-density correlations, a more convenient way is to analyze the two largest eigenvalues Λ_0 and Λ_1 of the transfer matrix using iDMRG in the sector with the same particle number. The density-density correlation length is then given by $\xi=2/\ln(\Lambda_0/\Lambda_1)$, and the phase transition occurs when ξ diverges, i.e., when $\Lambda_1\to\Lambda_0$.

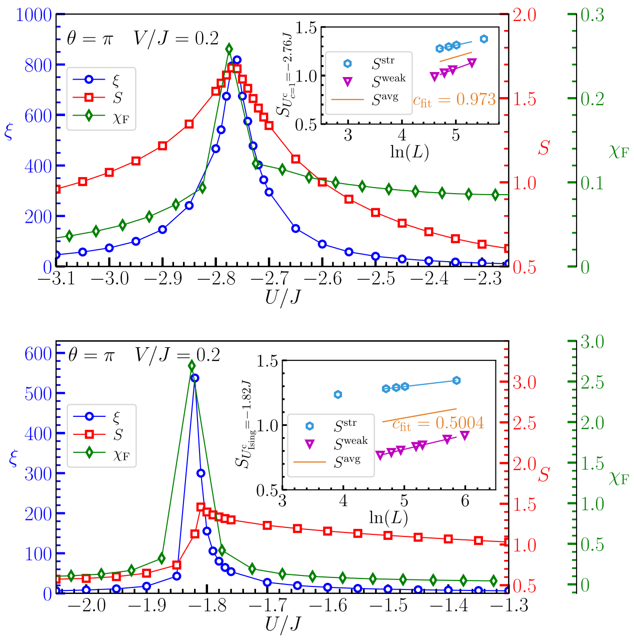

FIG. 5. Correlation length ξ, entanglement entropy S, and fidelity susceptibility χ_{F} as a function of U at $V=0.2J$ and $\theta=\pi$ from iDMRG ($M=800$), showing a $c=1$ transition for CDW-dimer at $U^{\mathrm{c}}_{c=1}=-2.76J$ (upper) and an Ising transition for dimer-Mott at $U^{\mathrm{c}}_{\mathrm{Ising}}=-1.82J$ (lower). Insets: entanglement entropy scaling from finite size DMRG at the transition points as a function of $\ln(L)$ according to Eq. (A3).

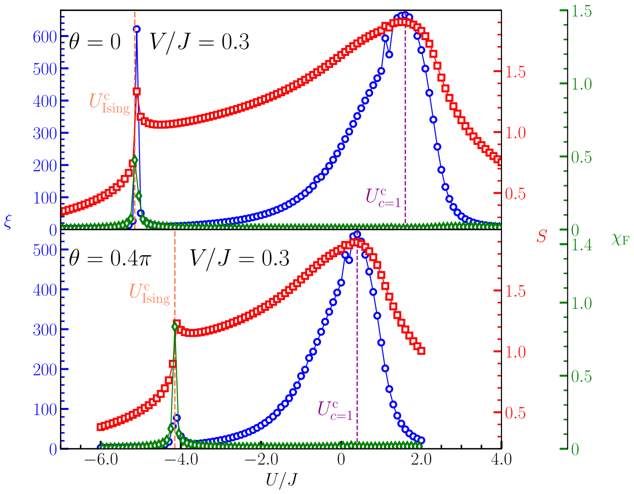

FIG. 6. iDMRG data for correlation length ξ, entanglement entropy S, and fidelity susceptibility χ_F for $V = 0.3J$ as a function of U. For $\theta = 0$ (top), the CDW to HI transition is at $U^c_{\rm Ising} = -5.15J$, and the HI to Mott transition is at $U^c_{c=1} = 1.6J$. For $\theta = 0.4\pi$ (bottom), $U^c_{\rm Ising} = -4.15J$, $U^c_{c=1} = 0.4J$.

In Fig. 5 we compare all three quantities at $\theta = \pi$ to illustrate the behavior for the CDW to dimer transition (upper) and the dimer to Mott transition (lower). All quantities have sharp maxima at the phase transition line, which agree within the parameter spacing of the simulations. In addition, the scaling in Eq. (A3) can be used to characterize the nature of the transition as shown in the insets, which give $c = 0.5004$ and $c = 0.973$ consistent with Ising and $c = 1$ transitions, respectively.

In Fig. 6 the analogous analysis is made for $\theta = 0$ (upper) and $\theta = 0.4\pi$ (lower), which show the CDW to HI and the HI to Mott transitions. In the latter case the maxima of S and ξ are broader, while χ_F is overall smaller but with a relatively sharp feature (for an enlarged scale see Fig. 7). In fact, we find that χ_F remains always sharp even as other maxima broaden for smaller V, as illustrated in Fig. 7. Hence, we obtain all data points for the phase diagrams from the maxima of χ_F only, but the maxima are always consistent with the other quantities.

Finally, we examine the effect of the number of states kept M, which plays the role of a cutoff, so the quantitative behavior directly at phase transitions may crucially depend on M. Hence, for the scaling of Eq. (A3) shown in the insets of Fig. 5 a large value $M = 800$ was used. However, for the *location* of the maxima, the value of M is much less important as illustrated in Fig. 8 where the $M = 800$ data points are on top of points with lower M except for $M = 50$. We find that using $M = 100$ allows for a good sampling of transition points in parameter space and gives identical values as $M = 800$ as checked at selected points.

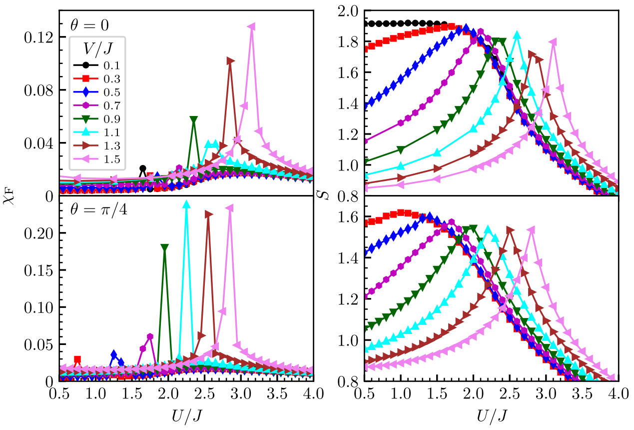

FIG. 7. Fidelity susceptibility χ_F (left) and entanglement entropy S (right) from iDMRG plotted as a function of U at the Mott to HI transition for $\theta = 0$ (upper) and $\theta = \pi/4$ (lower) and different V (legend applies to all subfigures).

Appendix B: Superfluid phases—In the bosonic limit ($\theta = 0$), the phase diagram exhibits a SF-PSF phase transition that has attracted interest in dimension $d = 1$ [77–79] and higher [79–83] due to its unusual Ising quantum critical point characterized by a $U(1) \times Z_2$ conformal field theory with fractional central charge $c = 3/2$. For corresponding gapless phases in the spin-1 chain see Ref. [39]. In the 1D model there is no breaking of the continuous U(1) symmetry, but quasi long-range order exists, which is characterized by algebraically decaying pair correlations $\langle (\hat{b}_i^\dagger)^2 (\hat{b}_{i+j})^2 \rangle$ in both phases. On the other hand the single particle correlation $\langle \hat{b}_i^\dagger \hat{b}_{i+j} \rangle$ decays exponentially in the PSF phase but remains long range in the SF phase, which we confirmed numerically [40]. Both superfluid phases require $K_+ > 2$, while the $(-)$ sector of the continuum Hamiltonian in Eq. (7) is always gapped. Consequently, all phase transitions between the superfluid and insulating phases are driven by the g_1 interaction and are of BKT type.

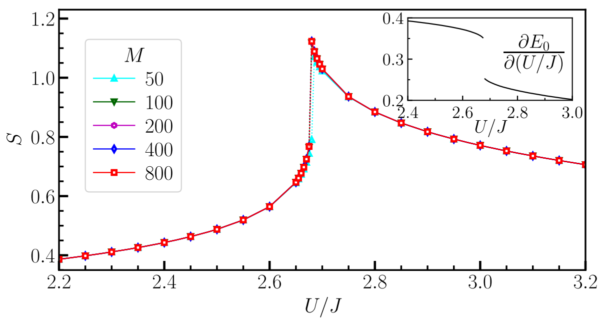

FIG. 8. Entanglement entropy S and derivative of ground-state energy E_0 (inset) over U for $V = 3J$, $\theta = \pi$. The jump at $U = 2.68J$ indicates a first order CDW-Mott transition.

The two distinct superfluid phases (SF and PSF) correspond to different locked values of the fields Φ_- and Θ_- depending on the value of K_- [39]. The correlation functions characterize the different gapless phases for $K_+ > 2$. For the slowly varying part of the single particle function we find [40]

$$\langle \hat{b}_0^\dagger \hat{b}_j \rangle_{\text{uni}} \simeq \frac{1}{2}\left(\langle \hat{S}_{1,0}^- \hat{S}_{1,j}^+ \rangle_{\text{uni}} + \langle \hat{S}_{2,0}^- \hat{S}_{2,j}^+ \rangle_{\text{uni}} \right) \propto |x|^{-\frac{1}{2K_+}} \left(\langle e^{i\sqrt{\pi}\Theta_-(0)} e^{-i\sqrt{\pi}\Theta_-(x)} \rangle + \text{H.c.} \right), \quad \text{(B1)}$$

where only the leading asymptotic behavior is retained. Generally, in the $(-)$ sector there is a competition between the g_2 and g_3 interactions which have scaling dimensions K_- and $1/K_-$, respectively. For $K_- > 1$, the Θ_--field is locked at $\Theta_- = 0$. In this case, the expectation values involving the vertex operators of Θ_- contribute a constant to the prefactor of $\langle \hat{b}_0^\dagger \hat{b}_j \rangle_{\text{uni}}$, so the single-particle function decays as a power law, which is the hallmark of the SF phase. However, for $K_- < 1$, we have $\Phi_- = 0$, while Θ_- fluctuates freely, resulting in an exponential decay of the single particle function. Hence, the change of single particle decay and the SF-PSF transition is determined by $K_- = 1$. The pair-superfluid phase in Fig. 3 is pushed to smaller values of V by the CDW phase, which we attribute to the g_4 interaction in Eq. (7) in combination with the pinned field $\Phi_- = 0$. For larger V and $K_+ < 2$ the HI-CDW Ising transition is also characterized by $K_- = 1$ as discussed above and therefore is in line with the SF-PSF transition, resulting again in a multicritical point where two gapless and two gapped phases meet, consistent with the numerical data in the inset of Fig. 3 for $\theta = 0$. Note that the slowly varying part of the pair correlation does not depend on Θ_-:

$$\langle (\hat{b}_0^\dagger)^2 (\hat{b}_j)^2 \rangle_{\text{uni}} \simeq \langle \hat{S}_{1,0}^- \hat{S}_{2,0}^- \hat{S}_{1,j}^+ \hat{S}_{2,j}^+ \rangle_{\text{uni}} \propto \langle e^{i\sqrt{4\pi}\Theta_+(0)} e^{-i\sqrt{4\pi}\Theta_+(x)} \rangle \propto |x|^{-\frac{2}{K_+}}. \quad \text{(B2)}$$

It remains algebraically decaying in either gapless phase as confirmed numerically [40].

For numerically locating the gapless to gapped BKT phase transitions, we use the level spectroscopy approach [64–70] where finite-size transition points are identified using excited energy level degeneracies, which are then extrapolated to the thermodynamic limit using exact diagonalization on periodic finite size systems. Figure 9 shows the relevant energy level crossing as a function of V. In the inset the corresponding crossings for different finite L are extrapolated to an infinite system size, which determines one SF/HI transition point to an accuracy of $0.01J$. This procedure is repeated for a large number of different values of U to obtain the insets of Fig. 3.

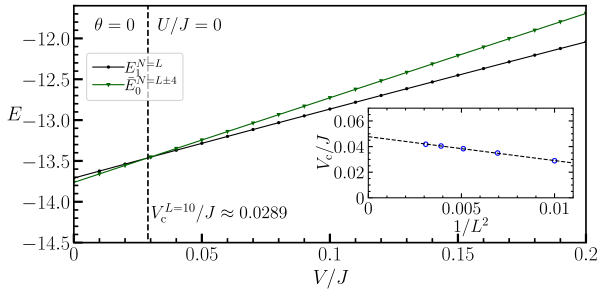

FIG. 9. Crossing of energy levels that represent the SF phase (green symbols) and the HI phase (black symbols). E_n^N denotes the energy of the nth excitation of the N-particle sector. Inset: extrapolation to $L \to \infty$.

Supplemental material for
Anyonic phase transitions in the 1D extended Hubbard model with fractional statistics

Martin Bonkhoff,[1,2] Kevin Jägering,[1] Shijie Hu,[1,3] Axel Pelster,[1] Sebastian Eggert,[1] and Imke Schneider[1]

[1] *Physics Department and Research Center OPTIMAS, University of Kaiserslautern-Landau, 67663 Kaiserslautern, Germany*

[2] *Theoretische Physik, Univ. Hamburg, Jungiusstr. 9, 20255 Hamburg, Germany*

[3] *Beijing Computational Science Research Center, Beijing 100193, China*

(Dated: June 12, 2025)

In the Supplemental material details about the lattice gauge function, the bosonization of the lattice model, the symmetry transformations, and additional numerical data are presented.

I. LATTICE GAUGE FUNCTION

With the restriction of a maximum of two particles per site, the Bosonic creation operator can be expressed exactly in terms of spin-1 operators. In the representation by triplet states of two spin-1/2 operators the corresponding expression is given by [1, 2]

$$\hat{b}_l^\dagger = \frac{\hat{S}^-_{1,l}}{\sqrt{2}}\left(a(0) + d(0)\hat{S}^z_{2,l}\right) + \frac{\hat{S}^-_{2,l}}{\sqrt{2}}\left(a(0) + d(0)\hat{S}^z_{1,l}\right) \tag{1}$$

where $a(\theta) = (1 + \sqrt{2}e^{i\theta})/2$ and $d(\theta) = (1 - \sqrt{2}e^{i\theta})$. We will now derive how this representation is affected by the multiplication with a density dependent phase factor, i.e. we will derive the form of $\hat{b}_l^\dagger e^{i\theta \hat{n}_l}$. The density-dependent phase decomposes as $e^{i\theta(\hat{n}_l - 1)} = e^{-i\theta \hat{S}^z_{1,l}} e^{-i\theta \hat{S}^z_{2,l}}$ where the exponentials of spin-1/2 operators can be expressed in terms of trigonmetric functions

$$e^{-i\theta \hat{S}^z_{n,l}} = \cos\left(\frac{\theta}{2}\right) \mathrm{id} - 2i \sin\left(\frac{\theta}{2}\right) \hat{S}^z_{n,l} \tag{2}$$

for $n = 1, 2$. We further notice that

$$\left(a(\tilde{\theta}) + d(\tilde{\theta})\hat{S}^z_{n,l}\right)\left(\cos\left(\frac{\theta}{2}\right) - 2i\sin\left(\frac{\theta}{2}\right)\hat{S}^z_{n,l}\right) = e^{-\frac{i\theta}{2}}\left(a(\tilde{\theta} + \theta) + d(\tilde{\theta} + \theta)\hat{S}^z_{n,l}\right) \tag{3}$$

for arbitrary angles $\tilde{\theta}$ and θ. Multiplication of the Boson operator with the density dependent phase therefore gives

$$\hat{b}_l^\dagger e^{i\theta \hat{n}_l} = \frac{\hat{S}^-_{1,l}}{\sqrt{2}}\left(a(\theta) + d(\theta)\hat{S}^z_{2,l}\right) + \frac{\hat{S}^-_{2,l}}{\sqrt{2}}\left(a(\theta) + d(\theta)\hat{S}^z_{1,l}\right) \quad . \tag{4}$$

In conclusion, on the level of spin-1/2 operators the action of the density dependent phase is solely reflected in the coefficients $a(\theta)$ and $d(\theta)$. It is straight-forward to check that this expression yields the correct matrix elements in the local Hilbert space of 3 states. It also can be used to verify the lattice gauge function in Eq. (6) of the main text.

II. BOSONIZATION

A. Mode expansion and Bosonization of spin operators

For the bosonization we follow the standard approach by first using the Jordan-Wigner mapping

$$\hat{S}^+_{q,l} = \hat{c}^\dagger_{q,l} \exp\left(i\pi \sum_{l'<l} \hat{n}_{q,l'}\right), \quad \hat{S}^z_{q,l} = \hat{n}_{q,l} - \frac{1}{2} \tag{5}$$

to a Fermionic representation where $\hat{c}^{\dagger}_{q,l}$ creates a Fermion on site l in chain $q = 1, 2$ and $\hat{n}_{q,l} = \hat{c}^{\dagger}_{q,l}\hat{c}_{q,l}$. We then take the continuum limit and project the Fermionic fields onto states with momentum near the Fermi points $\pm k_F$. This leads to right- and left-moving components in the mode expansion:

$$\hat{c}_{q,l} \to \sqrt{a}\left(\hat{\Psi}^q_R(x)e^{ik_F x} + \hat{\Psi}^q_L(x)e^{-ik_F x}\right) \tag{6}$$

where $x = a\,l$ and a is the lattice constant. Next, we apply the standard Bosonization formula [3]

$$\hat{\Psi}^q_{R/L}(x) = \frac{1}{\sqrt{2\pi a}}e^{i\sqrt{\pi}(\Theta_q(x)\pm\Phi_q(x))} \tag{7}$$

with the dual Bosonic fields Θ_q and Φ_q which fulfill $[\Phi_q(x), \Theta_{q'}(x')] = \frac{i}{2}\delta_{q,q'}\mathrm{sgn}(x - x')$. Here, the length scale a also serves as the ultraviolet energy cutoff of the theory. The dual Bosonic fields can be decomposed into right- and left-moving fields $\Phi_q = \phi_{R,q} + \phi_{L,q}$ and $\Theta_q = \phi_{R,q} - \phi_{L,q}$. We use the following mode expansions of these fields

$$\phi_{R,q}(x,t) = \phi^0_{R,q} + \hat{Q}_{R,q}\frac{x - vt}{L} + \phi^+_{R,q}(x,t) + \phi^-_{R,q}(x,t) \tag{8}$$

$$\phi_{L,q}(x,t) = \phi^0_{L,q} + \hat{Q}_{L,q}\frac{x + vt}{L} + \phi^+_{L,q}(x,t) + \phi^-_{L,q}(x,t) \tag{9}$$

for finite system size L and periodic boundary conditions where

$$\phi^-_{R,q}(x,t) = (\phi^+_{R,q}(x,t))^\dagger = \sum_n \frac{1}{\sqrt{4\pi n}}e^{i\frac{2\pi n}{L}(x - vt)}b^q_{R,n} \tag{10}$$

$$\phi^-_{L,q}(x,t) = (\phi^+_{L,q}(x,t))^\dagger = \sum_n \frac{1}{\sqrt{4\pi n}}e^{-i\frac{2\pi n}{L}(x + vt)}b^q_{L,n} \quad . \tag{11}$$

The Bosonic modes $b^q_{R,n}$ and $b^q_{L,n}$ fulfill the canonical commutation relations $[b^q_{R/L,n}, b^{q\,\dagger}_{R/L,n'}] = \delta_{n,n'}$ if taken from the same branch, otherwise they commute. The commutation rules for the zero modes are $[\phi^0_{R,q}, \phi^0_{L,q}] = \frac{i}{4}$ and $[\phi^0_{R,q}, \hat{Q}_{R,q}] = -\frac{i}{2}$ and $[\phi^0_{L,q}, \hat{Q}_{L,q}] = \frac{i}{2}$ such that the anti-commutation rules for the Fermion fields are ensured. For the Bosonic fields it follows

$$[\phi^-_{R/L,q}(x,t), \phi^+_{R/L,q}(y,0)] = -\frac{1}{4\pi}\ln\left(1 - e^{\pm i\frac{2\pi}{L}(x - y \mp vt)}e^{-\frac{2\pi}{L}a}\right) \tag{12}$$

where we have again used the short distance cutoff a to generate convergence. Using Baker-Cambell-Hausdorff $e^A e^B = e^{A+B}e^{\frac{1}{2}[A,B]}$ the vertex operators are normal-ordered:

$$\frac{1}{\sqrt{2\pi a}}\,e^{i\sqrt{4\pi}\,\phi_{R/L,q}(x)} = \frac{1}{\sqrt{L}}e^{i\sqrt{4\pi}\,\phi^+_{R/L,q}(x)}e^{i\sqrt{4\pi}\,\phi^-_{R/L,q}(x)} \quad . \tag{13}$$

The spin operator $S^z_{q,l} = \hat{n}_{q,l} - 1/2 =: \hat{n}_{q,l} :$ can now be bosonized using

$$:\hat{n}_{q,l}: \simeq a\left[\hat{\Psi}^{q\dagger}_R(x)\hat{\Psi}^q_R(x + a) + \hat{\Psi}^{q\dagger}_L(x)\hat{\Psi}^q_L(x + a) + (-1)^{\frac{x}{a}}\left(\hat{\Psi}^{q\dagger}_R(x)\hat{\Psi}^q_L(x) + \hat{\Psi}^{q\dagger}_L(x)\hat{\Psi}^q_R(x)\right)\right] \quad . \tag{14}$$

For the operator product expansion of two Fermion operators of the same branch we find

$$\begin{aligned}\hat{\Psi}^{q\dagger}_{R/L}(x)\hat{\Psi}^q_{R/L}(x + a) =& \frac{1}{L} : e^{\mp i\sqrt{4\pi}\,\phi_{R/L,q}(x)} :: e^{\pm i\sqrt{4\pi}\,\phi_{R/L,q}(x+a)} : \\ \approx& \mp\frac{i}{2\pi a} : e^{\mp i\sqrt{4\pi}\left(\phi_{R/L,q}(x) - \phi_{R/L,q}(x+a)\right)} : \\ =& \frac{1}{2\pi a}\left[\mp i + a\sqrt{4\pi}\,\frac{\partial\phi_{R/L,q}(x)}{\partial x} + a^2\sqrt{\pi}\,\frac{\partial^2\phi_{R/L,q}(x)}{\partial x^2}\right. \\ & \left.\pm ia^2 2\pi\left(\frac{\partial\phi_{R/L,q}(x)}{\partial x}\right)^2 + \mathcal{O}(a^3)\right]\end{aligned} \tag{15}$$

whereas the rapidly oscillating product of two Fermion operators of different branches is given by

$$(-1)^{\frac{x}{a}}\left(\hat{\Psi}^{q\dagger}_R(x)\hat{\Psi}^q_L(x)+\hat{\Psi}^{q\dagger}_L(x)\hat{\Psi}^q_R(x)\right) = \frac{(-1)^{\frac{x}{a}}}{2\pi a}e^{-2\pi[\phi^0_{R,q},\phi^0_{L,q}]}e^{-i\sqrt{4\pi}\Phi_q(x)}+\text{H.c.} \tag{16}$$

$$= \frac{(-1)^{\frac{x}{a}}}{2\pi a}e^{-i\frac{\pi}{2}}e^{-i\sqrt{4\pi}\Phi_q(x)}+\text{H.c.} \tag{17}$$

$$= -\frac{(-1)^{\frac{x}{a}}}{\pi a}\sin 2\sqrt{\pi}\,\Phi_q(x). \tag{18}$$

In leading order this results in

$$\hat{S}^z_{q,l}\simeq\frac{a}{\sqrt{\pi}}\frac{\partial\Phi_q(x)}{\partial x}-\frac{(-1)^{\frac{x}{a}}}{\pi}\sin\left(2\sqrt{\pi}\,\Phi_q(x)\right)\quad . \tag{19}$$

For the spin raising operator we get

$$\hat{S}^+_{q,l}\simeq e^{-i\sqrt{\pi}\Theta_q(x)}\left[b+\tilde{b}(-1)^{\frac{x}{a}}\sin\left(2\sqrt{\pi}\,\Phi_q(x)\right)\right] \tag{20}$$

where b and $\tilde{b}$ are non-universal constants. Note that the phases in the oscillating terms of Eqs. (19) and (20) depend on the treatment of zero modes where other conventions are possible [3].

B. Bosonization of hopping with dynamic gauge fields

In this section we determine the bosonized expression for the correlated hopping including the density-dependent phase. Our starting point is the spin-1/2 two-leg ladder model from Eq. (5) in the main text

$$H_{\text{kin}}=-\frac{1}{2}\sum_l\left[\tilde{t}\left(\hat{S}^z_{2,l},\hat{S}^z_{2,l+1}\right)\hat{S}^-_{1,l}\hat{S}^+_{1,l+1}+\tilde{t}\left(\hat{S}^z_{2,l},\hat{S}^z_{1,l+1}\right)\hat{S}^-_{1,l}\hat{S}^+_{2,l+1}+1\leftrightarrow 2+\text{H.c.}\right]$$

with the lattice gauge function

$$\tilde{t}(\hat{S}^z_{i,l},\hat{S}^z_{j,l+1})=\tilde{J}+J_z\hat{S}^z_{i,l}+\bar{J}_z\hat{S}^z_{j,l+1}+J_{zz}\hat{S}^z_{i,l}\hat{S}^z_{j,l+1} \tag{21}$$

for $i,j=1,2$ which we have derived in the main text with $\tilde{J}=\frac{J}{4}(1+\sqrt{2})(1+\sqrt{2}e^{i\theta})$ and higher spin interaction constants $J_z=\frac{J}{2}(1+\sqrt{2})(1-\sqrt{2}e^{i\theta})$, $\bar{J}_z=\frac{J}{2}(1-\sqrt{2})(1+\sqrt{2}e^{i\theta})$, and $J_{zz}=J(1-\sqrt{2})(1-\sqrt{2}e^{i\theta})$. We proceed by first bosonizing the free hopping and the gauge function separately and then performing operator-product expansions between the hopping and the lattice gauge terms whenever necessary. As the lattice gauge function is complex-valued we thereby need to consider the operator product expansions between the hermitian conjugated pairs of the hopping and the lattice gauge explicitly. After the Jordan-Wigner transformation the kinetic energy reads

$$H_{\text{kin}}=-\frac{1}{2}\sum_l\left[t^\star\left(\hat{n}_{2,l},\hat{n}_{2,l+1}\right)\hat{c}^\dagger_{1,l}\hat{c}_{1,l+1}+t^\star\left(\hat{n}_{2,l},\hat{n}_{1,l+1}\right)\hat{c}^\dagger_{1,l}\hat{c}_{2,l+1}+1\leftrightarrow 2+\text{H.c.}\right]$$

where

$$t(\hat{n}_{i,l},\hat{n}_{j,l+1})=\tilde{J}+J_z:\hat{n}_{i,l}:+\bar{J}_z:\hat{n}_{j,l+1}:+J_{zz}:\hat{n}_{i,l}::\hat{n}_{j,l+1}: \tag{22}$$

for $i,j=1,2$ and * denotes complex conjugation while $:\ldots:$ stands for normal ordering by subtracting the ground state expectation value. The Fermionic bilinears for $k_F=\frac{\pi}{2a}$ are given by

$$\begin{aligned}\hat{c}^\dagger_{q,l}\hat{c}_{q,l+1}\simeq i\,a\Big[&\hat{\Psi}^{q\,\dagger}_R(x)\hat{\Psi}^q_R(x+a)-\hat{\Psi}^{q\,\dagger}_L(x)\hat{\Psi}^q_L(x+a)\\&-(-1)^{\frac{x}{a}}\left(\hat{\Psi}^{q\,\dagger}_R(x)\hat{\Psi}^q_L(x+a)-\hat{\Psi}^{q\,\dagger}_L(x)\hat{\Psi}^q_R(x+a)\right)\Big]\end{aligned} \tag{23}$$

and are bosonized similarly to the local density in the previous subsection. In particular, we use Eq. (15) to determine the uniform contribution and proceed analogously to Eq. (18) for the oscillating contribution. The result (before taking the Hermitian conjugate) reads

$$\hat{c}^\dagger_{q,l}\hat{c}_{q,l+1}\simeq\frac{1}{\pi}+i\frac{a}{\sqrt{\pi}}\frac{\partial\Theta_q(x)}{\partial x}-\frac{a^2}{2}\left[\left(\frac{\partial\Theta_q(x)}{\partial x}\right)^2+\left(\frac{\partial\Phi_q(x)}{\partial x}\right)^2\right]-\frac{(-1)^{\frac{x}{a}}}{\pi}\cos\left(2\sqrt{\pi}\,\Phi_q(x)\right). \tag{24}$$

Note the different phase of the oscillating contribution compared to the local density. For the Bosonization of the gauge function we use $:\hat{n}_{q,l} := \hat{S}^z_{q,l}$ in Eq. (19) and evaluate the product $:\hat{n}_{q,l}::\hat{n}_{q,l+1}:$ by performing further operator product expansions. For the cross terms the following expressions are useful [4]

$$\frac{\partial\Phi_q(x)}{\partial x}\sin(2\sqrt{\pi}\Phi_q(x+a)) \simeq -\sin(2\sqrt{\pi}\Phi_q(x))\frac{\partial\Phi_q(x+a)}{\partial x} = \frac{1}{\sqrt{\pi}\,a}\cos(2\sqrt{\pi}\Phi_q(x)) \tag{25}$$

and

$$\sin\left(2\sqrt{\pi}\Phi_q(x)\right)\sin\left(2\sqrt{\pi}\Phi_q(x+a)\right) \simeq \frac{1}{2} - a^2\pi\left(\frac{\partial\Phi_q(x)}{\partial x}\right)^2 - \frac{1}{2}\cos\left(4\sqrt{\pi}\Phi_q\right) \quad . \tag{26}$$

Altogether, we find

$$\begin{aligned} :\hat{n}_{q,l}::\hat{n}_{q,l+1}: \simeq{}& \frac{a^2}{\pi}\left(\frac{\partial\Phi_q(x)}{\partial x}\right)^2 + \frac{2a(-1)^{\frac{x}{a}}}{\sqrt{\pi}\pi}\frac{\partial\Phi_q(x)}{\partial x}\sin\left(2\sqrt{\pi}\Phi_q(x+a)\right) \\ &- \frac{1}{\pi^2}\sin\left(2\sqrt{\pi}\Phi_q(x)\right)\sin\left(2\sqrt{\pi}\Phi_q(x+a)\right) \end{aligned} \tag{27}$$

$$\begin{aligned} \simeq{}& \frac{a^2}{\pi}\left(\frac{\partial\Phi_q(x)}{\partial x}\right)^2 + \frac{2(-1)^{\frac{x}{a}}}{\pi^2}\cos\left(2\sqrt{\pi}\Phi_q(x)\right) \\ &- \frac{1}{\pi^2}\left(\frac{1}{2} - a^2\pi\left(\frac{\partial\Phi_q(x)}{\partial x}\right)^2 - \frac{1}{2}\cos\left(4\sqrt{\pi}\Phi_q\right)\right) \end{aligned} \tag{28}$$

which can be summarized as

$$:\hat{n}_{q,l}::\hat{n}_{q,l+1}: = -\frac{1}{2\pi^2} + \frac{2a^2}{\pi}\left(\frac{\partial\Phi_q(x)}{\partial x}\right)^2 + \frac{2(-1)^{\frac{x}{a}}}{\pi^2}\cos\left(2\sqrt{\pi}\Phi_q(x)\right) + \frac{1}{2\pi^2}\cos\left(4\sqrt{\pi}\Phi_q\right) \quad . \tag{29}$$

The different contributions to the correlated intra-chain hopping

$$\hat{\mathcal{K}}^{\text{intra}}_{l,l+1} \equiv -\frac{1}{2}\left(t^\star\left(\hat{n}_{2,l},\hat{n}_{2,l+1}\right)\hat{c}^\dagger_{1,l}\hat{c}_{1,l+1} + t^\star\left(\hat{n}_{1,l},\hat{n}_{1,l+1}\right)\hat{c}^\dagger_{2,l}\hat{c}_{2,l+1} + \text{H.c.}\right) \tag{30}$$

$$= \hat{\mathcal{K}}^a_{l,l+1} + \hat{\mathcal{K}}^b_{l,l+1} + \hat{\mathcal{K}}^c_{l,l+1} \tag{31}$$

can now be determined by direct multiplication. Here, we have defined

$$\hat{\mathcal{K}}^a_{l,l+1} \equiv -\frac{1}{2}\sum_{q=1,2}\left(\tilde{J}^\star\hat{c}^\dagger_{q,l}\hat{c}_{q,l+1} + \text{H.c.}\right) \tag{32}$$

$$\hat{\mathcal{K}}^b_{l,l+1} \equiv -\frac{1}{2}\sum_{q=1,2}\left[\hat{c}^\dagger_{q,l}\hat{c}_{q,l+1}\left(J^\star_z:\hat{n}_{\bar{q},l}: + \bar{J}^\star_z:\hat{n}_{\bar{q},l+1}:\right) + \text{H.c.}\right] \tag{33}$$

$$\hat{\mathcal{K}}^c_{l,l+1} \equiv -\frac{1}{2}\sum_{q=1,2}\left[J^\star_{zz}\hat{c}^\dagger_{q,l}\hat{c}_{q,l+1}:\hat{n}_{\bar{q},l}::\hat{n}_{\bar{q},l+1}: + \text{H.c.}\right] \tag{34}$$

where $\bar{q}=1$ if $q=2$ and $\bar{q}=2$ if $q=1$. Since the evaluation of these terms only involves multiplication of fields with different chain indices we do not need to perform further operator product expansions. We obtain

$$\hat{\mathcal{K}}^a_{l,l+1} = \sum_{q=1,2}\left\{\frac{a^2\text{Re}(\tilde{J})}{2}\left[(\partial_x\Theta_q)^2 + (\partial_x\Phi_q)^2\right] - \frac{a\,\text{Im}(\tilde{J})}{\sqrt{\pi}}\,\partial_x\Theta_q\right\} \tag{35}$$

$$\begin{aligned} \hat{\mathcal{K}}^b_{l,l+1} = \sum_{q=1,2}\Bigg[&-\frac{a\,\text{Re}(J_z+\bar{J}_z)}{\pi\sqrt{\pi}}\,\partial_x\Phi_q - \frac{a^2}{\pi}\text{Im}(J_z+\bar{J}_z)\partial_x\Theta_q\partial_x\Phi_{\bar{q}} \\ &-\frac{\text{Re}(J_z-\bar{J}_z)}{\pi^2}\cos\left(2\sqrt{\pi}\Phi_q\right)\sin\left(2\sqrt{\pi}\Phi_{\bar{q}}\right)\Bigg] \end{aligned} \tag{36}$$

$$\begin{aligned} \hat{\mathcal{K}}^c_{l,l+1} = \sum_{q=1,2}\Bigg[&-\frac{2a^2\text{Re}(J_{zz})}{\pi^2}\left(\partial_x\Phi_q\right)^2 + \frac{2\text{Re}(J_{zz})}{\pi^3}\cos\left(2\sqrt{\pi}\Phi_q\right)\cos\left(2\sqrt{\pi}\Phi_{\bar{q}}\right) \\ &-\frac{\text{Re}(J_{zz})}{2\pi^3}\cos\left(4\sqrt{\pi}\Phi_q\right)\Bigg] \quad . \end{aligned} \tag{37}$$

We further introduce '+' and '-' - fields

$$\Phi_\pm = \Phi_1 \pm \Phi_2, \quad \Theta_\pm = (\Theta_1 \pm \Theta_2)/2 \tag{38}$$

which yields

$$\hat{\mathcal{K}}^a_{l,l+1} = \frac{a^2 \mathrm{Re}(\tilde{J})}{2}\left[2\left(\partial_x\Theta_+\right)^2 + \frac{1}{2}\left(\partial_x\Phi_+\right)^2 + 2\left(\partial_x\Theta_-\right)^2 + \frac{1}{2}\left(\partial_x\Phi_-\right)^2\right] - \frac{2a\,\mathrm{Im}(\tilde{J})}{\sqrt{\pi}}\,\partial_x\Theta_+ \tag{39}$$

$$\begin{aligned}\hat{\mathcal{K}}^b_{l,l+1} =& -\frac{a\,\mathrm{Re}(J_z+\bar{J}_z)}{\pi\sqrt{\pi}}\,\partial_x\Phi_+ - \frac{a^2\,\mathrm{Im}(J_z+\bar{J}_z)}{\pi}\left[\partial_x\Theta_+\partial_x\Phi_+ + \partial_x\Theta_-\partial_x\Phi_-\right]\\ &+ \frac{\mathrm{Re}(J_z-\bar{J}_z)}{\pi^2}\sin\left(2\sqrt{\pi}\Phi_+\right)\end{aligned} \tag{40}$$

$$\begin{aligned}\hat{\mathcal{K}}^c_{l,l+1} =& -\frac{a^2\mathrm{Re}(J_{zz})}{\pi^2}\left[\left(\partial_x\Phi_+\right)^2 + \left(\partial_x\Phi_-\right)^2\right]\\ &+ \frac{2\mathrm{Re}(J_{zz})}{\pi^3}\left[\cos\left(2\sqrt{\pi}\Phi_+\right) + \cos\left(2\sqrt{\pi}\Phi_-\right) - \frac{1}{2}\cos\left(2\sqrt{\pi}\Phi_+\right)\cos\left(2\sqrt{\pi}\Phi_-\right)\right] \ .\end{aligned} \tag{41}$$

Here, we omitted oscillating terms and contributions of higher order. The additional constant in Eq. (29) entering $:\hat{n}_{l,q}::\hat{n}_{l+1,q}:$ can be absorbed into the hopping amplitude of $\hat{\mathcal{K}}^a_{l,l+1}$, i.e. $\tilde{J} \to \tilde{J} - J_{zz}/2\pi^2$. Altogether, the intra-chain hopping is given by

$$\begin{aligned}\hat{\mathcal{K}}^{\mathrm{intra}}_{l,l+1} \simeq& \frac{a^2\mathrm{Re}\left(\tilde{J} - \frac{J_{zz}}{2\pi^2}\right)}{2}\left[2\left(\partial_x\Theta_+\right)^2 + \frac{1}{2}\left(\partial_x\Phi_+\right)^2 + 2\left(\partial_x\Theta_-\right)^2 + \frac{1}{2}\left(\partial_x\Phi_-\right)^2\right]\\ &- \frac{a^2\mathrm{Re}(J_{zz})}{\pi^2}\left[\left(\partial_x\Phi_+\right)^2 + \left(\partial_x\Phi_-\right)^2\right] - \frac{a\,\mathrm{Re}(J_z+\bar{J}_z)}{\pi\sqrt{\pi}}\,\partial_x\Phi_+ - \frac{2a\,\mathrm{Im}(\tilde{J} - \frac{J_{zz}}{2\pi^2})}{\sqrt{\pi}}\,\partial_x\Theta_+\\ &- \frac{a^2\,\mathrm{Im}(J_z+\bar{J}_z)}{\pi}\left[\partial_x\Theta_+\partial_x\Phi_+ + \partial_x\Theta_-\partial_x\Phi_-\right]\\ &+ \frac{2\mathrm{Re}(J_{zz})}{\pi^3}\left[\cos\left(2\sqrt{\pi}\Phi_+\right) + \cos\left(2\sqrt{\pi}\Phi_-\right) - \frac{1}{2}\cos\left(2\sqrt{\pi}\Phi_+\right)\cos\left(2\sqrt{\pi}\Phi_-\right)\right]\\ &+ \frac{\mathrm{Re}(J_z-\bar{J}_z)}{\pi^2}\sin\left(2\sqrt{\pi}\Phi_+\right) \ .\end{aligned} \tag{42}$$

The operator $\sin(2\sqrt{\pi}\Phi_+)$ is not allowed by symmetry as discussed in section III. Hence, the lattice model can only realize coupling constants for which this operator has zero amplitude. In the following we will therefore exclude this operator.

The inter-chain hopping

$$\hat{\mathcal{K}}^{\mathrm{inter}}_{l,l+1} = -\frac{1}{2}\left(t^\star\left(\hat{n}_{2,l}, \hat{n}_{1,l+1}\right)\hat{c}^\dagger_{1,l}\hat{c}_{2,l+1} + t^\star\left(\hat{n}_{1,l}, \hat{n}_{2,l+1}\right)\hat{c}^\dagger_{2,l}\hat{c}_{1,l+1} + \mathrm{H.c.}\right) \tag{43}$$

is bosonized by returning to spin language and directly inserting the bosonized expressions for the spin operators, i.e. Eq. (20), into the spin flip terms. This results in

$$\hat{\mathcal{K}}^{\mathrm{inter}}_{l,l+1} \simeq -\frac{\mathrm{Re}(\tilde{J})}{\pi}\cos\left(2\sqrt{\pi}\Theta_-\right) \tag{44}$$

where we neglected further corrections caused by the gauge function which would only renormalize the prefactor in front of the $\cos(2\sqrt{\pi}\Theta_-)$-term but not generate further operator content.

C. Bosonization of density-density interactions and complete Hamiltonian

Finally, we consider the onsite and nearest neighbor interaction terms

$$\hat{H}_{\mathrm{int}} = \sum_l \sum_{q=1,2}\left[\frac{U}{2}:\hat{n}_{q,l}::\hat{n}_{\bar{q},l}: + V\left(:\hat{n}_{q,l}::\hat{n}_{q,l+1}: + :\hat{n}_{q,l}::\hat{n}_{\bar{q},l+1}:\right)\right] \ . \tag{45}$$

Bosonizing we obtain [3]

$$:\hat{n}_{q,l}::\hat{n}_{q,l+1}:\simeq -\frac{1}{2\pi^2}+\frac{2a^2}{\pi}\left(\partial_x\Phi_q\right)^2+\frac{1}{2\pi^2}\cos\left(4\sqrt{\pi}\Phi_q\right) \tag{46}$$

$$\begin{aligned}:\hat{n}_{q,l}::\hat{n}_{\bar{q},l'}:\simeq &\frac{a^2}{\pi}(\partial_x\Phi_q)(\partial_x\Phi_{\bar{q}})\\ &+\frac{-1+2\delta_{l,l'}}{2\pi^2}\Big[\cos\left(2\sqrt{\pi}(\Phi_q-\Phi_{\bar{q}})\right)-\cos\left(2\sqrt{\pi}(\Phi_q+\Phi_{\bar{q}})\right)\Big]\end{aligned} \tag{47}$$

for $l'=l,l+1$ where we have omitted oscillating contributions. Transforming into '+' and '-' - fields this yields

$$\begin{aligned}\hat{H}_{\rm int}\simeq &\int dx\Big\{\frac{a}{4\pi}\left[(U+6V)\left(\partial_x\Phi_+\right)^2-(U-2V)\left(\partial_x\Phi_-\right)^2\right]\\ &+\frac{U-2V}{2\pi^2 a}\left[-\cos\left(2\sqrt{\pi}\Phi_+\right)+\cos\left(2\sqrt{\pi}\Phi_-\right)\right]+\frac{V}{\pi^2 a}\cos\left(2\sqrt{\pi}\Phi_+\right)\cos\left(2\sqrt{\pi}\Phi_-\right)\Big\}\ .\end{aligned} \tag{48}$$

We are now in the position to add up all terms and arrive at the Bosonized Hamiltonian

$$\hat{H}\simeq\hat{H}_+ +\hat{H}_- +\hat{H}_{+-} \tag{49}$$

with

$$\begin{aligned}\hat{H}_+ &= \hat{H}^0_+ +\int dx\Big[A(\partial_x\Theta_+)+B(\partial_x\Phi_+)+\Delta(\partial_x\Theta_+)(\partial_x\Phi_+)+\frac{g_1}{(\pi a)^2}\cos(2\sqrt{\pi}\Phi_+)\Big], \qquad (50)\\ \hat{H}_- &= \hat{H}^0_- +\int dx\Big[\Delta(\partial_x\Theta_-)(\partial_x\Phi_-)+\frac{g_2}{(\pi a)^2}\cos(2\sqrt{\pi}\Phi_-)+\frac{g_3}{(\pi a)^2}\cos(2\sqrt{\pi}\Theta_-)\Big],\\ \hat{H}_{+-} &= \frac{g_4}{(\pi a)^2}\int dx\cos(2\sqrt{\pi}\Phi_+)\cos(2\sqrt{\pi}\Phi_-), \qquad (51)\end{aligned}$$

where $\hat{H}^0_\nu$ for $\nu=+,-$ denotes the ordinary Tomonaga-Luttinger Hamiltonian

$$\hat{H}^0_\nu=\frac{u_\nu}{2\pi}\int dx\left[K_\nu\left(\partial_x\Theta_\nu\right)^2+\frac{1}{K_\nu}\left(\partial_x\Phi_\nu\right)^2\right]\ . \tag{52}$$

We obtain for the Luttinger parameter to lowest order in the interactions

$$K_+=2\left(1+\frac{U+6V-4\,\mathrm{Re}(J_{zz})/\pi}{\pi\mathrm{Re}(\tilde{J}-J_{zz}/2\pi^2)}\right)^{-1/2}, \tag{53}$$

$$K_-=2\left(1-\frac{U-2V+4\,\mathrm{Re}(J_{zz})/\pi}{\pi\mathrm{Re}(\tilde{J}-J_{zz}/2\pi^2)}\right)^{-1/2} \tag{54}$$

while the velocities for each channel $\nu=+,-$ are given by

$$u_\nu=a\,2\pi\mathrm{Re}(\tilde{J}-J_{zz}/2\pi^2)/K_\nu\ . \tag{55}$$

Due to the asymmetry with respect to the Tomonaga-Luttinger basis we get linear couplings in the theory, i.e.

$$A=-\frac{2}{\sqrt{\pi}}\mathrm{Im}\left(\tilde{J}-\frac{J_{zz}}{2\pi^2}\right) \tag{56}$$

$$B=-\frac{1}{\pi\sqrt{\pi}}\mathrm{Re}(J_z+\bar{J}_z) \tag{57}$$

$$\Delta=-\frac{a}{\pi}\mathrm{Im}(J_z+\bar{J}_z) \tag{58}$$

which can be interpreted as chemical potentials for the density and phase-excitations for each sector as well as couplings proportional to the momentum operator of each liquid. The latter implies that we have chosen a reference frame, where the system is not at rest.

Symmetry	Lattice	Bosonic fields
Translation	$\hat{b}_j \to \hat{b}_{j+1}$	$\hat{\Phi}_+(x) \to \hat{\Phi}_+(x) + \sqrt{\pi}$, $\hat{\Theta}_+(x) \to \hat{\Theta}_+(x)$ $\hat{\Phi}_-(x) \to \hat{\Phi}_-(x)$, $\hat{\Theta}_-(x) \to \hat{\Theta}_-(x)$
Time reversal $\mathcal{K}$	$\hat{b}_j \to \hat{b}_j$	$\hat{\Phi}_+(x) \to \hat{\Phi}_+(x)$, $\hat{\Theta}_+(x) \to -\hat{\Theta}_+(x)$ $\hat{\Phi}_-(x) \to \hat{\Phi}_-(x)$, $\hat{\Theta}_-(x) \to -\hat{\Theta}_-(x)$
$U(1)$ gauge	$\hat{b}_j \to \hat{b}_j e^{i\alpha}$	$\hat{\Phi}_+(x) \to \hat{\Phi}_+(x)$, $\hat{\Theta}_+(x) \to \hat{\Theta}_+(x) - \alpha/\sqrt{\pi}$ $\hat{\Phi}_-(x) \to \hat{\Phi}_-(x)$, $\hat{\Theta}_-(x) \to \hat{\Theta}_-(x)$
Site parity $\mathcal{I}_-$	$\hat{b}_j \to \hat{b}_{-j}$	$\hat{\Phi}_+(x) \to -\hat{\Phi}_+(-x) + \sqrt{\pi}$, $\hat{\Theta}_+(x) \to \hat{\Theta}_+(-x)$ $\hat{\Phi}_-(x) \to -\hat{\Phi}_-(-x)$, $\hat{\Theta}_-(x) \to \hat{\Theta}_-(-x)$
Link parity $\mathcal{I}$	$\hat{b}_j \to \hat{b}_{1-j}$	$\hat{\Phi}_+(x) \to -\hat{\Phi}_+(-x)$, $\hat{\Theta}_+(x) \to \hat{\Theta}_+(-x)$ $\hat{\Phi}_-(x) \to -\hat{\Phi}_-(-x)$, $\hat{\Theta}_-(x) \to \hat{\Theta}_-(-x)$

TABLE I: Symmetry operations and their realizations in Bosonic fields.

The pinning terms that appear in our bosonized theory are given by the following coupling constants in the weak coupling limit

$$\frac{g_1}{a} = \frac{1}{2}(2V - U) + \frac{2}{\pi}\mathrm{Re}(J_{zz}), \tag{59}$$

$$\frac{g_2}{a} = \frac{1}{2}(U - 2V) + \frac{2}{\pi}\mathrm{Re}(J_{zz}), \tag{60}$$

$$\frac{g_3}{a} = -\pi\mathrm{Re}(\tilde{J}), \tag{61}$$

$$\frac{g_4}{a} = V - \frac{\mathrm{Re}(J_{zz})}{\pi} \quad . \tag{62}$$

It must be noted here that the mapping from bosons to spin operators already implies a finite interaction in terms of J_{zz}, which is non-zero even for $\theta = U = V = 0$. Therefore, the weak-coupling limit is never exact and the actual coupling constant will quantitatively differ from the formulas given above. Nonetheless, the operator content and the qualitative behavior with increasing θ, V and U is robust.

III. SYMMETRIES

Here we discuss how the symmetry transformations on the lattice Hamiltonian are reflected by symmetry operations on the fields in the bosonization as summarized in Table I. This will be used to identify which operators are allowed or forbidden in the effective field theory Hamiltonian.

The anyonic lattice model of interest $\hat{H} = \hat{H}_{\mathrm{kin}} + \hat{H}_{\mathrm{int}}$ with

$$\hat{H}_{\mathrm{kin}} = -J\sum_l \left[\hat{b}_l^\dagger \hat{b}_{l+1} e^{i\theta\hat{n}_l} + \mathrm{H.c.}\right] \tag{63}$$

$$\hat{H}_{\mathrm{int}} = \sum_l \left[\frac{U}{2}\hat{n}_l(\hat{n}_l - 1) + V\hat{n}_l\hat{n}_{l+1}\right] \tag{64}$$

exhibits translational invariance and conservation of total particle number ($U(1)$ gauge). Link reflection symmetry $\mathcal{I}$ and time-reversal $\mathcal{K}$, in contrast, are broken. All symmetries are inherited by the Bosonic low-energy description and Table I summarizes their realizations.

A modified inversion symmetry is still obeyed [5]. The lattice model is invariant under the combined symmetry operation $\tilde{\mathcal{I}} = \hat{U}(\theta)\mathcal{K}\mathcal{I}$ where the non-linear unitary transformation $\hat{U}(\theta) = e^{-i\theta\sum_l \hat{n}_l(\hat{n}_l - 1)/2}$ generates a density-dependent phase for Bosonic operators [5]

$$\hat{b}_l^\dagger \to \hat{U}(\theta)\hat{b}_l^\dagger\hat{U}^\dagger(\theta) = \hat{b}_l^\dagger e^{-i\theta\hat{n}_l} \quad . \tag{65}$$

While the realizations of $\mathcal{K}$ and $\mathcal{I}$ are known, see Table I, it is difficult to determine how the transformation $\hat{U}(\theta)$ acts on the Bosonic fields. This is due to the fact that the density dependent phase $\exp(-i\theta\hat{n}_l)$ is represented by integer values of n_l on the lattice, which ensures a $\theta \to \theta + 2\pi$ periodicity. In the continuum limit there is no such

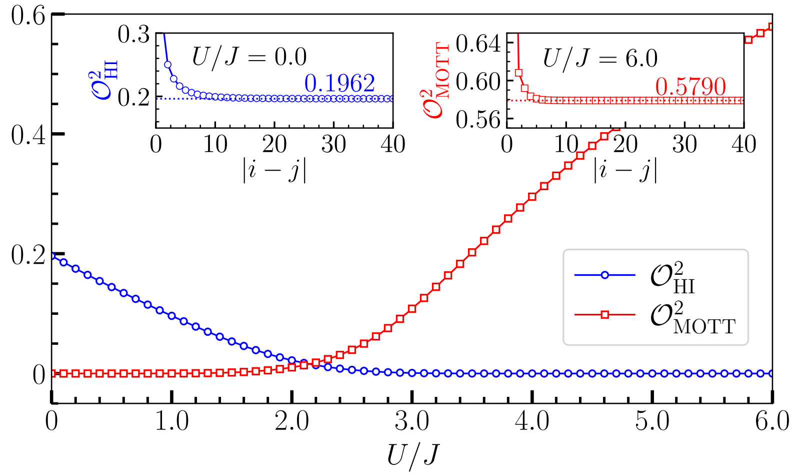

FIG. 1: String order parameters $\mathcal{O}^2_{\rm HI}$ and $\mathcal{O}^2_{\rm MOTT}$ plotted along the HI to Mott transition as a function of U, showing the existing string order in both phases at $V = J$ and $\theta = 0$. The insets show how the values were obtained for two typical parameters in the HI phase $U=0$ and the Mott phase $U=6J$, respectively. $\mathcal{O}(|i-j|)$ is extrapolated to $|i-j| \to \infty$ marked by the dotted lines. Data shown from finite DMRG, system size $L = 100$, bond dimension $M = 400$, periodic boundary conditions.

lattice restriction, so it is far from trivial to implement shifts of the fields that have this topological property. From Eq. (65) and section I we know that $\hat{U}(\theta)$ generates factors of the form as in Eq. (2) above which can be absorbed by redefinition of the coefficients $a(\theta)$ and $b(\theta)$ which in turn determine the coupling constants $\tilde{J}, J_z, \bar{J}_z$ and J_{zz} of the spin-1/2 two-leg ladder model. Such non-linear transformations cannot be tracked in the bosonized expressions of $\hat{S}^{\pm}_{q,l}$ in Eq. (20) and therefore the realization of the combined symmetry operation $\hat{U}(\theta)\mathcal{KI}$ in $\Theta_\pm$ is unclear.

On the other hand, it is clear that densities $\hat{b}^\dagger_l \hat{b}_l = \hat{n}_l = -\hat{S}^z_{1,l} - \hat{S}^z_{2,l} + 1$ are not affected by $\hat{U}(\theta)$, so therefore any transformation on the fields due to $\hat{U}(\theta)$ must also leave the spin-z operators in Eq. (19) invariant. Therefore, shifts on the Φ-fields cannot be generated by $\hat{U}(\theta)$, while we cannot make any statement how the Θ-fields are transformed.

Next, we turn to the modified inversion symmetry which is represented by the combined symmetry operation $\tilde{\mathcal{I}} = \hat{U}(\theta)\mathcal{KI}$. For densities in Eq. (19) this operation corresponds to a simple inversion symmetry $S^z_{q,l} \to S^z_{q,1-l}$, since $\mathcal{K}$ and $\hat{U}(\theta)$ do not affect the densities. We therefore conclude that the Bosonic Φ-fields transform as

$$\Phi_q(x) \to -\Phi_q(-x) \quad q = 1,2 \tag{66}$$

and

$$\Phi_+(x) \to -\Phi_+(-x), \quad \Phi_-(x) \to -\Phi_-(-x) \tag{67}$$

under the action of the combined symmetry $\hat{U}(\theta)\mathcal{KI}$. Even without knowing the symmetry action on the Θ-fields, the transformation property of $\Phi_+(x)$ in Eq. (67) rules out the existence of the $\sin(\sqrt{4\pi}\,\Phi_+(x))$ - operator as a perturbation. Note, that the operators $\Delta\partial_x\Theta_\pm(x)\partial_x\Phi_\pm(x)$ appearing in the bosonized anyonic Hamiltonian in Eq. (7) of the main text obey the combined $\mathcal{KI}$ symmetry, i.e. $\hat{\Phi}_\pm(x) \to -\hat{\Phi}_\pm(-x)$ and $\hat{\Theta}_\pm(x) \to -\hat{\Theta}_\pm(-x)$, see Table I.

IV. BEHAVIOR OF ORDER PARAMETERS

In this section we present further data for the order parameter. Fig. 1 shows the string order parameters $\mathcal{O}^2_{\rm MOTT}$ and $\mathcal{O}^2_{\rm HI}$ from Eqs. (18) and (20) in the main text plotted along the HI to Mott transition as a function of U, showing the existing string order in both phases at $V = J$ and $\theta = 0$. The insets show how the values were obtained for two typical parameters in the HI phase $U=0$ and the Mott phase $U=6J$, respectively. $\mathcal{O}(|i-j|)$ is extrapolated to $|i-j| \to \infty$ marked by the dotted lines. Here infinite DMRG with system size $L = 100$ and bond dimension $M = 400$ was used with periodic boundary conditions.

The order parameter that captures the specific long range nature order of the CDW phase is defined in Eq. (19) of the main text as

$$\mathcal{O}^2_{\rm CDW} = \lim_{|i-j|\to\infty} (-1)^{|i-j|} \langle \delta\hat{n}_i \delta\hat{n}_j \rangle \tag{68}$$

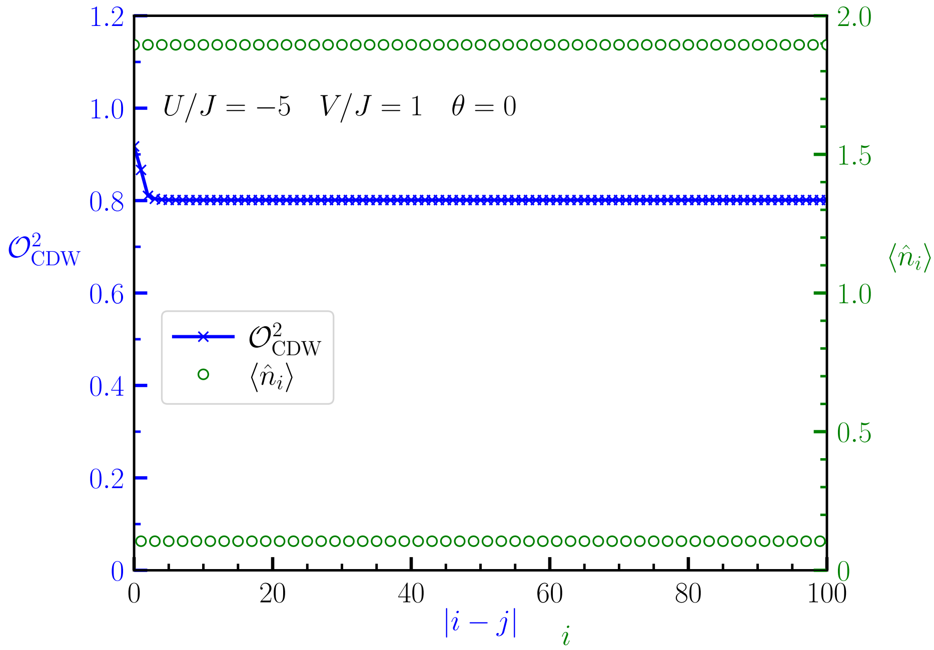

FIG. 2: The order parameter $\mathcal{O}^2_{\mathrm{CDW}}$ (blue symbols) and the local densities $\langle \hat{n}_i \rangle$ (green symbols) plotted as a function of site distance $|i-j|$ and the site i, respectively. Finite size DMRG with $L = 200$ and $M = 400$ with periodic and twisted boundary conditions was used to show that long range order in Eq. (68) and an alternating local density in Eq. (69) can be observed as order parameters of the CDW.

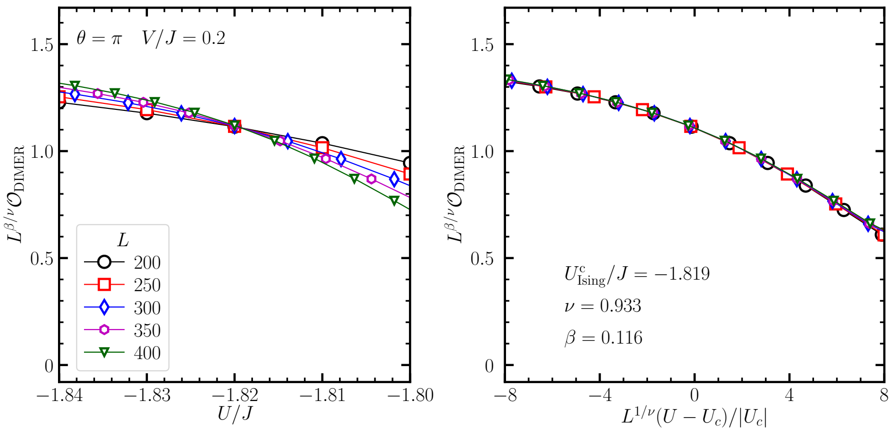

FIG. 3: Collapsing of data of the Dimer order parameter for various system sizes L at $\theta = \pi$ and $V/J = 0.2$. The DMRG data give a Dimer to Mott transition at $U^c_{\mathrm{Ising}}/J = -1.819$ with critical exponents $\nu = 0.933$ and $\beta = 0.116$ which are close to 1 and 1/8, respectively, in agreement with the $c = 1/2$ Ising universality class. Bond dimension $M = 400$.

with $\delta\hat{n}_i = \hat{n}_i - 1$. The blue crosses in Fig. 2 clearly show a non-decaying $\mathcal{O}^2_{\mathrm{CDW}}$ at long distances for a parameter point in the CDW phase. The breaking of the $\mathbb{Z}_2$ with respect to bond-centered inversion symmetry becomes manifest when considering the *local* order parameter defined by the density difference on neighboring sites in finite systems

$$\mathcal{O}_{\mathrm{CDW}} \propto |\langle \hat{n}_{\mathrm{even}} \rangle - \langle \hat{n}_{\mathrm{odd}} \rangle| \tag{69}$$

which can be alternatively used for a numerical analysis. The alternating behavior of the local density is depicted in green circles in Fig. 2.

Fig. 3 shows a finite size scaling analysis of the Dimer order parameter along the Dimer to Mott transition. The data collapse at the critical point yield critical exponents $\nu = 0.933$ and $\beta = 0.116$ which are close to 1 and 1/8, respectively, in agreement with the $c = 1/2$ Ising universality class.

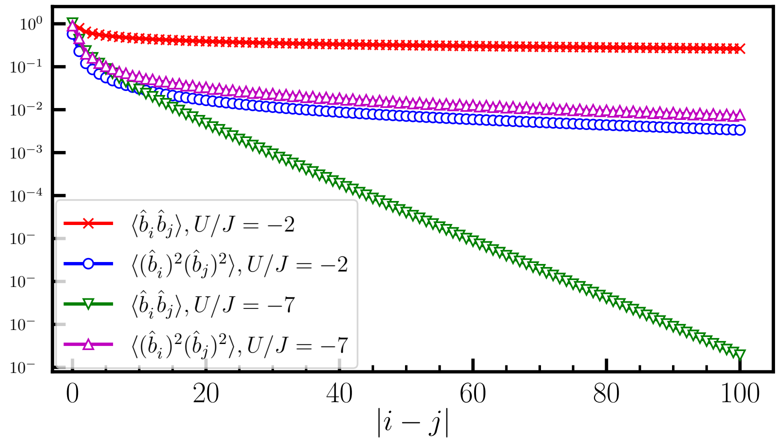

FIG. 4: Logarithmic plot of the single particle correlation and the pair correlation from DMRG ($L = 200, M = 500$) for $\theta = 0$ and $V = 0$, and two values of U showing algebraic decay (red, purple and blue data) compared to exponential decay (green data) that can be used to clearly distinguish the SF ($U = -2J$) and PSF ($U = -7J$) phases.

As discussed in the End Matter B, the order parameters of the superfluid phases are quasi long-range correlation functions. While both SF and PSF phases have algebraically decaying pair correlations, the single particle correlation is long range only in the SF phase, as shown in Fig. 4. This behavior was first discussed in Ref. [1] to distinguish different XY phases in spin-1 chains. While the quasi long-range order can be used to identify the different phases, it is also possible to use the fidelity susceptibility discussed in End Matter A to pinpoint the transition accurately. This is due to the fact that the transition takes place between two gapped phases in the $(-)$ sector as discussed in End Matter B.

[1] H. J. Schulz, Phys. Rev. B **34**, 6372 (1986), URL `https://link.aps.org/doi/10.1103/PhysRevB.34.6372`.

[2] M. Dalmonte, M. Di Dio, L. Barbiero, and F. Ortolani, Phys. Rev. B **83**, 155110 (2011), URL `https://link.aps.org/doi/10.1103/PhysRevB.83.155110`.

[3] T. Giamarchi, *Quantum Physics in One Dimension* (Clarendon Press, 2003).

[4] G. I. Japaridze and A. P. Kampf, Phys. Rev. B **59**, 12822 (1999), URL `https://link.aps.org/doi/10.1103/PhysRevB.59.12822`.

[5] F. Lange, S. Ejima, and H. Fehske, Phys. Rev. Lett. **118**, 120401 (2017), URL `https://link.aps.org/doi/10.1103/PhysRevLett.118.120401`.